University of Stavanger

FACULTY OF SCIENCE AND TECHNOLOGY

BACHELOR'S THESIS

Study programme/specialisation: Petroleum Engineering/Drilling and Well Technology	Spring semester, 2021 Open

Author:
Sveinung Huglen Bratten

Supervisor(s):
- Rune Wiggo Time
- Andrianifaliana Herimonja Rabenjafimanantsoa
- Hans Joakim Skadsem

Title of bachelor's thesis:
An experimental research of Newtonian fluids in an annular Heavy-Over-Light fluid displacement

Credits: 20

Keywords: Rayleigh-Taylor Instability, primary cementing, reverse circulation cementing, Reynolds number, Atwood number, Kelvin-Helmholtz instability, fluid instabilities, convection, advection, diffusion, flow velocity, fluid flow	Number of pages: 57 + supplemental material/other: 9 Stavanger, 31.05.2021

An experimental research of Newtonian fluids in an annular Heavy-Over-Light fluid displacement

by
Sveinung Huglen Bratten

Thesis submitted in fulfillment of the requirements for the degree of Bachelor

Universitetet i Stavanger

Faculty of Science and Technology
Department of petroleum Engineering
2021

Abstract

During the construction of a well, casings are considered essential for the well integrity. The job of securing the casing in place, i.e. the primary cementing of the casing, is a challenging task in itself due to the vast amount factors that come into play. There are several ways of cementing a case in place, but they all have the same main goal; to securely displace the drilling fluid and replace it with a heavier cement slurry. For the cement to be able to provide the best possible structural support, and to prevent any leakage, it is critical that it is not exposed to a large amount of mixing with another fluid. Reverse circulation is one of the techniques used today to ensure a good primary cementing. It has been proven[1] [2] that this method of displacement brings several benefits. It also provides us with a complex problem in which the heavier cement slurry is placed on top of the lighter drilling fluid.

In this study we will continue Camilla Bjørnsens (2020) work on density-unstable displacement of Newtonian fluid in an annular space. With an improved experimental setup and a larger interval of data we can confirm some of her work and also add new knowledge to the topic. With the use of a camera, density-unstable interfaces with an At of 0.0035, 0,01 and 0,02 in a system exposed to the outlet flow of 0, 10, 20, and 40mm/s has been documented. When keeping the Atwood number constant and only changing the flow rate, one can see that a larger flow rate introduces less backflow and overall mixing, as well as more time efficient displacement. The convection term of the system then seems to become the more dominant factor. When keeping the flow velocity constant, and changing the Atwood number, we see something interesting. At a lower Atwood number there seems to be less backflow than an increased Atwood number. This is due to the now heavier fluid sinking faster into the lighter fluid, pushing it back up. A higher Atwood number also seems to introduce more spin in an eccentric annulus. Similar to an increased flow velocity, an increase in the Atwood number will also result in a more time efficient displacement.

Acknowledgement

I would like to thank all parts who played a role in this project. This applies especially to my student team, consisting of PHD student Maryam, Ghorbani and Master student, Sjur Haugen Bjørlo, as well as my advisors, Professor Rune Wiggo Time, Senior Engineer Andrianifaliana Herimonja Rabenjafimanantsoa, and Associate Professor Hans Joakim Skadsem. Our meetings and exchange of ideas have played a major part in this thesis and the project as a whole. I would also like to thank my family and friends who have kept up my motivation through the 3 last years.

Last but not least I would also like to thank the Danish-American inventor, Niels Christensen, whose principal invention was the O-ring. Without his invention, the ongoing leakage from the experimental setup would surely have spiraled me into a dark place.

Contents

List of Figures

List of Tables

Nomenclature

At	Atwood number
D	Hydraulic depth
g	Gravitational constant
ID_C	Inner diameter of cylinder
ID_P	Inner diameter of pipe
Re	Reynolds number
KHI	Kelvin-Helmholtz Instability
RTI	Rayleigh-Taylor Instability
v	Flow velocity
u	Flow velocity
D_H	Hydraulic diameter
m	Mass
P,p	Pressure
ρ	Density
ρ_1	Density of heavy fluid
ρ_2	Density of light fluid
d_2	Diameter of large pipe
d_1	Diameter of smallest pipe
μ	Viscosity
∇	Gradient differential operator
HPG	Hydrostatic Pressure Gradient
τ	Shear stress
γ	Shear rate
L	length
Q	Flow rate
T, t	Time
β	Inclination
HOL	Heavy-Over-Light
s	Second(s)
$Z_k(t)$	penetration depth after a given time
α_k	Constant independent of At

Chapter 1

Introduction

1.1 Background

During a drilling operation one will have to stabilize the well at certain points to ensure it's integrity. For each section that is drilled a casing will have to be lowered into the borehole. The casing is essentially a large diameter pipe whose objective is to protect both the well and the formation from any external or internal forces or reactions that might lead to damages. It is therefore crucial that the casing is installed in the best possible manner. This is normally done by pumping cement slurry down the drillpipe and forcing it in to the annulus between the casing and formation. The drilling fluid has to be displaced and replaced with cement slurry as best as possible to ensure there are no leakage to the surface, to seal the well, and to provide structural support for the casing [3].

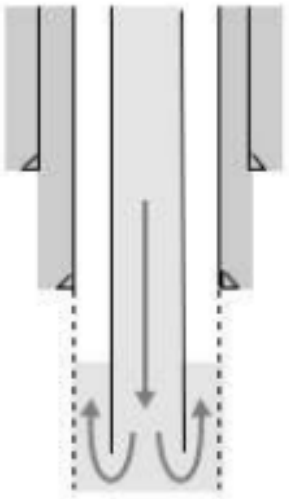

Figure 1.1: Conventional cementing

However, if one were to encounter a weaker formation, this way of displacing cement slurry may create a larger risk of formation damage due to the high circulation pressure. In this case "reverse circulation method" might be a better option. The concept of reverse circulation method lies somewhat in the name itself. Instead of pumping cement slurry down through the drillpipe and then up through the annulus, it is pumped directly into the annulus. This will result in a lower circulation pressure, making it safer to introduce in a weak formation area. According to Kurus and Seatters (2005) paper on RCPC (Reverse Circulation Primary Cementing) [1], this lower circulation pressure allows cement placement with no apparent losses. This can be somewhat credited to the reverse circulation methods possibility of higher flow rate, denser cement slurry and a higher cement column.

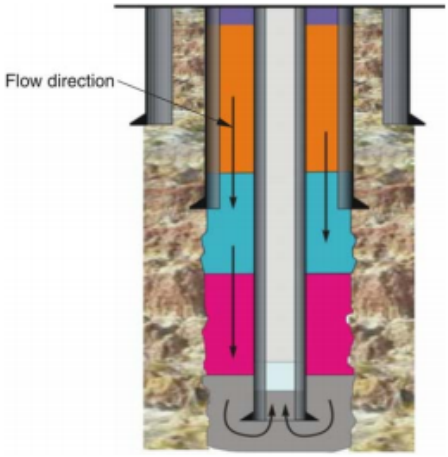

Figure 1.2: Reverse circulation method [4]

Prior to cementing the annulus is filled with drilling fluid to ensure pressure against the formation wall. This is essential for the integrity of the well. On the other hand this will also result in a natural instability, in which the heavier cement slurry and spacer are placed on top of the lighter drilling fluid. By heavier we mean a higher density. This instability is known as the Rayleigh-Taylor instability, after Lord Rayleigh and G.I. Taylor. Due to the buoyancy force, which is dependent on the density, the lighter fluid will start to rise to the top, and the heavier fluid will start to sink through the lighter fluid. Unless the system of heavy-over-light is affected by an external factor, such as an outlet flow or an change in hydrostatic pressure, the growing "chaos" withing the system will result in unwanted mixing of the fluids.

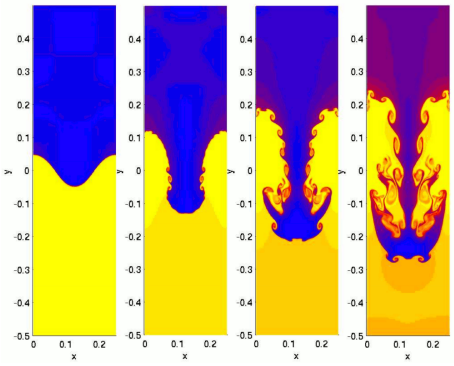

Figure 1.3: Growth of chaos in RT-instability [5]

Although the growth of the chaos and change of flow in the system has a complex description, it has been done both theoretically and experimentally

several times before. However, there are not many experiments using the geometry of a drillstring. The application of such experiments onto said geometry is therefore questionable. As explained in Bjørnsens (2020) [3] thesis on "Reverse Heavy Over Light", more studies are needed on this topic.

1.2 Statement and objective of problem

To achieve a better understanding of a HOL system we need more investigation on the topic as well as confirmation of earlier research. In this thesis the aim is therefore to confirm Camilla Bjørnsens result in her thesis on HOL from 2020, as well as improving her setup to achieve clearer results. It will also look into the movement of the fluid front.
Will a higher flow velocity lead to a better displacement in a HOL system?
Will it do the same with an increased Atwood number?
By answering such questions we can narrow down more of the knowledge gap surrounding this topic, which allows for a more efficient and to some extent safer primary cementing operations. All in all the objectives of this thesis will be to:

- Collect a larger and clearer spectrum of data showing the reaction of a HOL fluid arrangement in an annular space.
- Apply different outlet flow rates and different Atwood numbers to see how it affects the displacement of light fluid.
- Investigate the movement of the fluid front in an annular space.

1.3 Limits and safety factors within the project

The fluids used in this experiment are Newtonian fluids, such as fresh water and distilled water mixed with salt, and either red colorant or black ink. Also, the flow that is applied to the system is laminar. It is therefore important to note that in a situation using non-Newtonian fluid, such as drilling fluid and cement slurry the results may vary. One should also note that the thesis does not include any information regarding secondary cementing operations. The outlet flow itself is not affected by any pumps, as it is only dependent on the opening of the valve and the pressure created by the height of the fluid column.

Due to the ongoing pandemic of Covid-19 all participants in the projects were to use face masks at all times. During the execution of the experiments in the older setup and the construction of the newer setup, a fall hazard was present. A safety harness attached to a rigid surface was therefore used several times while climbing.

1.4 Execution of experiments and structure of thesis

This thesis mostly contains experimental results together with some prior literature research. The further improvements of Bjørnsens setup and the experiments themselves have been conducted together with my student team consisting of; PHD student, Maryam Ghorbani, and Master student, Sjur Haugen Bjørlo. They will write their own theses on the topic.

The thesis has already started with chapter 1, introduction. It gives a brief explanation of the background, statement of problem, objective of thesis, limits, safety factors, and also about the execution of the experiments. Moving on to chapter 2, the theory. Here one will find a more detailed explanation of the theoretical foundation needed to complete the experiments and to understand the results. This chapter is heavily dependent of the literature review. In chapter 3, the methodology; how we conducted our experiments, what equipment was use, and an overview of the experimental setup. Chapter 4 contains all the results and any discussion surrounding the results. In chapter 5 the conclusion can be found together with my recommendations on further work. At the end of the thesis there's a list of references followed by Appendix A, B,C, and D.

Chapter 2

Theory

2.1 Primary cementing and well design

Primary cementing is an important step during any drilling operation. For each section that is drilled through the formation a casing must be cemented in place. For the cement to have the desired effect, i.e. to give structural support for the well and prevent any leakage to and from the formation, it needs to fully displace the drilling fluid to remain as "clean" as possible (not mixed with other fluids).

To get applicable results we want to reduce the amount of external factors. The experimental setup was therefore built somewhat proportionally similar to what one would see in a more realistic well design (See 3.1 and 3.2). Typically a $9^5/_8$"($\simeq 245mm$) production casing is used in a mature water-flooded field [6]. The hole section in which this casing is placed in is $12^1/_4$". The remaining space between outside of the casing and the inside of the wellbore is therefore $2^5/_8$"($\simeq 667mm$). For deeper and more high pressure wells, a smaller production casing and production liner might be used.
The production casing is used to isolate production zones and contain formation pressures. It may also sometimes be exposed to injection pressures from fracture jobs, gas lift, or water injection support [6]. It is therefore critical that this section receives a good primary cementing job.

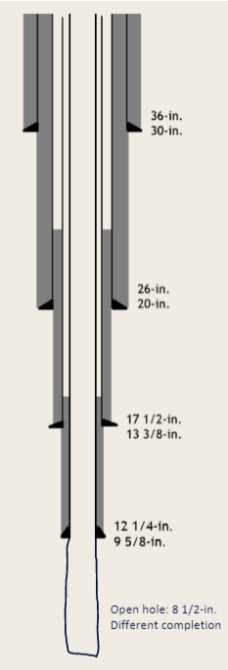

Figure 2.1: Typical dimensions of borehole and casing [7]

A poor primary cement job could have serious consequences for production, well integrity, and ultimately human life. Poor primary cement jobs are the lead cause of off-shore well blow outs [8]. Some examples are the Deepwater Horizon blow-out in Gulf of Mexico (2010) and the blow-out in Montara, western Australia (2009). Although the blow-out at Deepwater Horizon can be blamed at a series of events, the initial cause was a poor primary cement job [9].

2.1.1 Conventional circulation VS Reverse-circulation method

Normally to cement a casing in place cement slurry is pumped down into the tubing and further pushed up through the annulus, fully displacing the empty space between the casing and the formation itself. This is known as the more conventional method of cementing. There are several different operations one can use to complete such a method of cementing. The most commonly used cementing operation in a drilling process is *single stage cementing* [10]. Which drilling process that is used varies depending on the length of the casing string or if the formation cannot support the hydrostatic pressure of the column of cement [11].

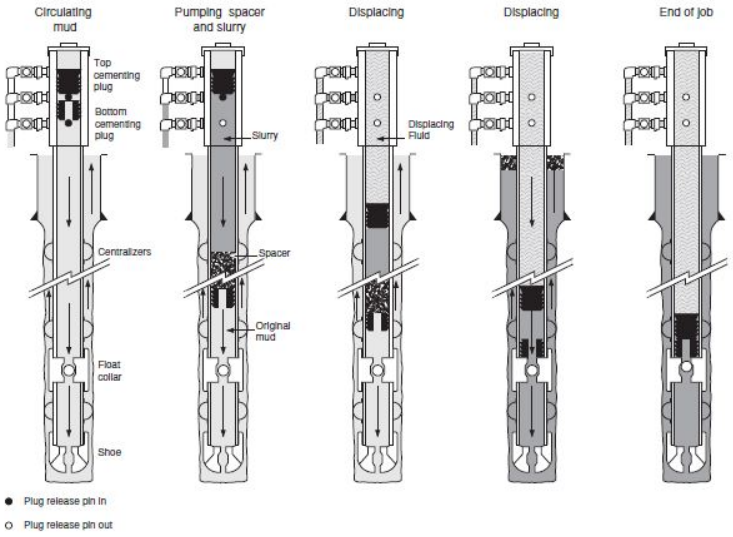

Figure 2.2: Single stage cementing operation [11]

In situations where the formation above the casing shoe are in danger of breaking down due to high ECD(equivalent circulating density), a better way of displacing cement slurry is needed. When using the reverse-circulation technique the cement slurry is pumped down the annulus and displaces the drilling fluid back up through the casing. Much of the equipment used in conventional cementing has to be modified to be used in the reverse-circulation method [4]. According to [2], [12], and [1] the reverse circulation method allows for a wider range of cement slurry compositions. As a result of this, heavier or more-retarded cement can be placed at the lower portion of casing, and lighter or accelerated cement can be placed at the top of the annulus. To determine the necessary volume of cement needed and to minimize overplacement, a caliper survey should be conducted before starting cementing procedure. A caliper survey will also help to detect any geometrical deviation which can negatively affect the flow of product [13]. Reverse Circulation method is not something new. It has been used for a longer period of time, both offshore and on land wells where one has access to the annulus. In Palacio, Gardner, Delabroy and Govil paper (2020) [14] one can read an analysis of the cement quality in casing sections after spending 30 years in the Norwegian north sea. In this case the reverse cementing method was not used to reduce the friction pressure. Due to a weak zone midway up the open hole section the method was used as a step 2 after conventional cementing (step 1) up to the weak zone.

2.1.2 Eccentricity

When creating a well you want the annulus to be as symmetrical as possible. Although a perfect symmetrical geometry is not very realistic, any deviation from this will lead to a more unequal displacement of fluid. If a casing is placed more towards one side of the wellbore the annulus becomes *eccentric*. The deviation from a perfectly centered annulus is known as the *eccentricity* or *standoff*. The larger the standoff the more centered the casing is with respect to the wellbore. The smaller the standoff the more unequal the annulus becomes - the casing is closer to one side than the other. This will effect the total displacement as the heavy fluid will follow the path with least resistance, i.e. the widest part [15]. Figure 2.3 2.4 [16] shows how a smaller standoff will effect the displacement of the fluid. Note that in figure 2.4 the direction of the flow is from the bottom and up, i.e. a more conventional cementing. With a reverse cementing method and an unstable density hierarchy the fluid displacement is more unpredictable.

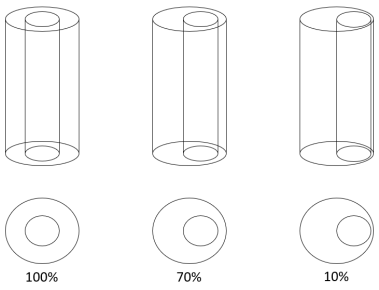

Figure 2.3: Different intensities of standoff

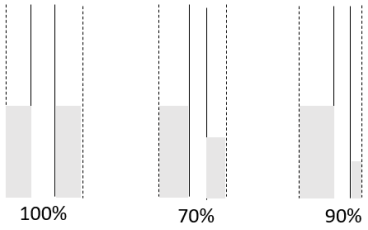

Figure 2.4: Effect of different standoffs

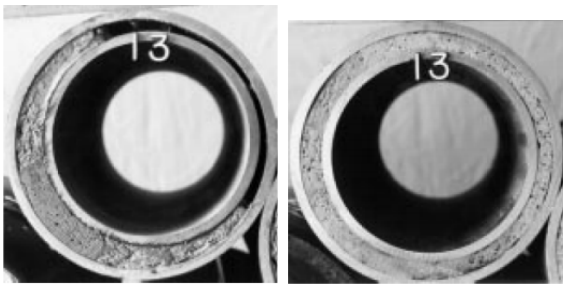

(a) (b)

Figure 2.5: a) Poor placement and low stand-off , b) Good placement and high stand-off [17]

2.2 Fundamentals of fluid properties

In this project one of the goals is to study and understand more of fluid instabilities in an annular geometry. Describing such instabilities can be complex, and one must therefore first understand some of the fundamentals of the fluids behavior.

2.2.1 Density

Density is a measure of mass per unit volume of a given material. When using SI-units the units describing density is often kg/m^3 or g/m^3. The latter one is what is used for this project.
Density is often denoted with the letter ρ, and can be calculated with the following formula:

$$Density = \frac{Mass}{Volume}$$

which can be denoted as,

$$\rho = \frac{M}{V} \tag{2.1}$$

2.2.2 Atwood number (At)

The Atwood number is a dimensionless number which describes the relation between the densities of two fluids. Because fluid stability is highly dependent on the Atwood number, it has been very much used in the study of fluid behavior, and can therefore also be found at several points throughout this paper. The formula used to find the Atwood number is:

$$At = \frac{\rho_1 - \rho_2}{\rho_1 + \rho_2} \tag{2.2}$$

In an open geometry (square), the outer edges of the mixing zone (HOL fluid arrangement) seems to follow the large time asymptotic scaling law [18]. The Atwood number can therefore be used to calculate the penetration distance of heavy-fluid bubbles into the light fluid as a function of acceleration time scale,

$$Z_k(t) = (-1)^k \cdot \alpha_k \cdot At \cdot g \cdot t^2 \tag{2.3}$$

- $Z_k(t)$ = penetration depth after a given time
- α_k = Constant independent of At. Measured experimentally and is often found to be around 0.6 [19]

2.2.3 Rheology

Rheology is the study of the deformation and flow of matter (liquid, solid, gas) (Aurélie Taguet, 2020). From the rheological properties we can classify different fluids after their flow behavior. More spesifically, we can classify them in what "Newtonian fluid" and "non-newtonian fluid".

Newtonian fluids have a viscosity that is not affected by the shear rate (which again is proportional to the shear stress). Although no real liquid fits the definition of Newtonian liquid completely, we say that liquids that do not contain particles larger than molecules, such as water, oil and glycols, can be assumed as Newtonian liquids (for simplicity). *Non-Newtonian fluids* however are dependent on the shear rate and are therefore either "shear thickening" og "shear thinning". A fluid that is shear thickening will have it's viscosity increasing as a result of an increase in share rate. The opposite, a fluid that is shear thinning, will have it's viscosity declining due to the increase of the share rate. Most drilling fluid that are used today are shear thinning.

On figure 2.1 one can see how a newtonian fluid behaves to shear rate and shear stress, together with some of the most famous fluid description models. Here one can also see that for see that not all fluids have a shear stress that starts at origin. This is due to some fluids ability to behave like gel when exposed to no flow over time. The gel strength will have a yield point at which it will start to behave like a fluid again.

Although the use of Non-Newtonian fluids are not present in these experiments, it is important to note that such fluid will have a different behavior, and may therefore vary from any results that are collected in experiments found in this thesis.

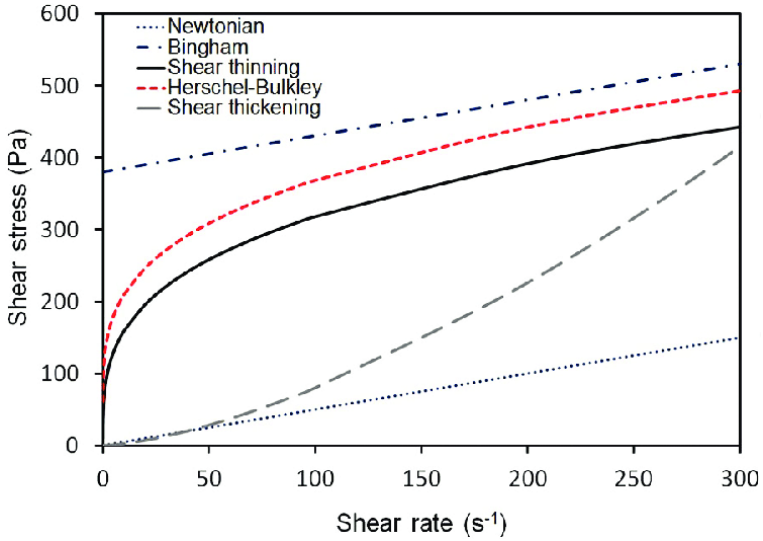

Figure 2.6: Shear rate versus shear stress for newtonian and non-newtonian fluid

2.2.4 Viscosity:

Viscosity is an important measurement within the research of rheology, as it describes the fluids resistance to flow. The higher the viscosity the more external force has to be applied to the fluid to achieve flow (yield stress). A realistic displacement of fluids in a primary cementing operation will contain fluid with a higher viscosity. Viscosity (μ) is defined as the ratio between shear stress (τ) and the shear rate (γ).

$$\mu = \frac{\tau}{\gamma} \tag{2.4}$$

Viscosity is also very temperature dependent. In liquid the increase of temperature usually decreases the viscosity. In contrast to gases there are no microscopic theory surrounding the viscosity of liquid [20]. In these experiments we are using the viscosity of water at 20°C = 1.0016mPa = 1.0116cP [21] Further research is necessary to apply a more realistic viscosity to a HOL-system.

2.2.5 Reynolds number (Re)

Reynolds number is a dimensionless number which helps describe the flow pattern of a fluid. The associated correlation of the Reynolds number will vary after which rheological model is being used. [22] It also varies after which geometry is being used. In the experiments conducted for this thesis, Newtonian fluid was used in a annulus geometry. The correct formula for the Reynolds number with such rheology and such geometry is:

$$Re = \frac{(\frac{\rho_1+\rho_2}{2}) \cdot v \cdot (d_2 - d_1)}{\mu} \tag{2.5}$$

- ρ_1 = Density of heavy fluid
- ρ_2 = Density of light fluid
- $\frac{\rho_1+\rho_2}{2}$ = Average density of fluid front
- v = velocity
- d2 = Diamaeter of largest pipe
- d1 = Diameter of smallest pipe
- μ = viscosity

The higher the Reynolds number the closer to a turbulent flow regime it gets. To avoid mixing of fluids a more laminar flow is For displacing cement we do not want. For a pipe the different types of flow regimes in respect to the Reynolds number are defined as:

Table 2.1: Classification of flow regimes with respect to Reynolds number in a pipe geometry

Flow type	Range of Reynolds number
Laminar Flow	Re $\leq$ 2300
Transient Flow	2300 $<$ Re $<$ 4000
Turbulent Flow	Re $\geq$ 4000

Note that this classification of flow regimes may vary depending on the fluid and geometry that is used.

2.2.6 Froude number (Fr)

The Froude number is a dimensionless value which describes different flow regimes of open channel flow. The Froude number is a ratio of the inertial and gravitational forces. The Froude number can be calculated from this equation [23]:

$$Fr = \frac{V}{\sqrt{g \cdot D}} \tag{2.6}$$

Where:
V = Fluid velocity,
D = Hydraulic depth (cross sectional area of flow divided by top width),
g = Gravitational acceleration.

From the Froude number that is calculated one can understand how the fluid moves through the referenced cros sectional area.
However, when used in the context of Boussinesq approximation, i.e. buoyancy-driven flows, we get a densimetric Froude number. It can be calculated from the following equation:

$$Fr = \frac{V}{\sqrt{g \cdot At \cdot D}} \tag{2.7}$$

$Fr < 1$, system is dominated by buoancy forces (density difference). Also known as subcrtical flow.
Fr = 1, critical flow. Flow velocity is equal to wave propagation.
$Fr > 1$, supercritical. Flow velocity is faster than wave propagation.

2.3 Continuity equation

Fluids must move in such a way that mass is conserved. The statement of mass conservation is called the continuity equation. The continuity equation is an equation describing the transport of a given quantity. There is a very general continuity equation that can be altered and applied to a variety of physical phenomenas. In this case, for fluid dynamics, the continuity equation states that the same amount of mass that enters the system must also leave the system plus the accumulation of fluid gathered within the system.[24]

$$\frac{\partial \rho}{\partial t} + \nabla \cdot (\rho u) = 0 \tag{2.8}$$

For a homogeneous and incompressible fluid, such as Newtonian fluid, $\rho 1 = \rho 2$. The continuity equatifon for such a fluid then becomes:

$$\nabla \cdot \vec{u} \tag{2.9}$$

2.4 Navier-Stokes equations

The Navier-Stokes equations are a set of partial differential equations describing the motion of viscous fluids. They are an extensions of the Euler Equations and include the effects of viscosity on the flow. [25] They express the conservation of mass and momentum for Newtonian fluids. However, the Navier-Stokes equations are mainly a statement of the balance of momentum. For it to be able to fully describe the flow of a fluid, additional information, such as conservation of mass, balance of energy, and/or an equation of state, is needed. This is why the *continuity equation* plays an important role in the Navier-Stokes equations.

In modern notation, the Navier-Stokes equation is: [26]

$$\frac{\partial \vec{u}}{\partial t} + \vec{u} \cdot \nabla \vec{u} = -\frac{\nabla P}{\rho} + \mu \cdot \nabla^2 \cdot \vec{u} \tag{2.10}$$

If we consider fluid in a pipe with a hydrostatic pressure gradient, we get:

$$\frac{\partial \vec{u}}{\partial t} + \underbrace{\vec{u} \cdot \nabla \vec{u}}_{\text{Convection}} = -\frac{\nabla P}{\rho} + \underbrace{\mu \cdot \nabla^2 \cdot \vec{u}}_{\text{Viscous dissipation}} + \underbrace{\rho g \vec{i}_y}_{\text{HPG}} \tag{2.11}$$

In the last term (Hyrdostatic Pressure Gradient) $\vec{i}$ is a unit vector in y-directon, i.e. the direction of the gravitational acceleration. If the pipe that contains the fluid were to change it's angle the term for the hydrostatic pressure gradient can be denoted as, $\rho g \beta$, where β is the angle of inclination [3]. Note also the *convection* and *diffusion/viscous dissipation* term in (2.11). Together with *advection* they represent important descriptions of the flow:

- Convection - The collective motion of particles in a fluid. A flow that comvines advection and diffusion
- Advection - The motion of particles along the bulk flow. Advection requires already motion in the fluid, and cannot occur in solid materials [3]
- Diffusion - the net movement of particles from high concentration to low concentration.

2.5 Rayleigh-Taylor and Kelvin-Helmholtz Instability

The *Rayleigh-Taylor instability (RTI)* is a gravity driven density unstable system, where a heavier fluid is placed on top of a lighter fluid. It is a dynamic process in which the two fluids seek to reduce their combined potential energy [27]. Any disturbance of the interface between these fluids will cause the heavier fluid to spike down through the lighter fluid, and in return the lighter fluid will be pushed upwards through the heavier fluid, often in bubble-like shapes. The perturbation progress will develop from a linear growth at the very start before going over to non-linear growth, resulting in the spikes and plumes that can be seen on the figure below.

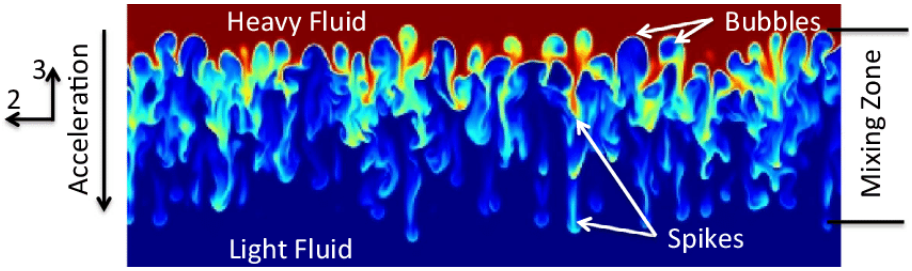

Figure 2.7: Early stages of RTI [28]

The mixing of the two fluids result in a turbulent flow at the interface. According to Sharp, D.H. [28] the RTI follows four main stages:

a) Perturbation amplitudes are small compared to their wavelengths. One can linearize the equation of motion, resulting in an exponential growth of the instability.

b) Non-linear effects begin to appear and the formation of mushroom-shaped spikes can be observed. In this stage the mushroom structures seems to have a constant growth rate.

c) The spikes and bubbles will start to interact with each other. Larger bubbles will start to appear as the smaller bubbles are enveloped by larger ones.

d) Growth of bubbles and break-up of spikes will be seen until eventually the region has a completely turbulent flow/mixing.

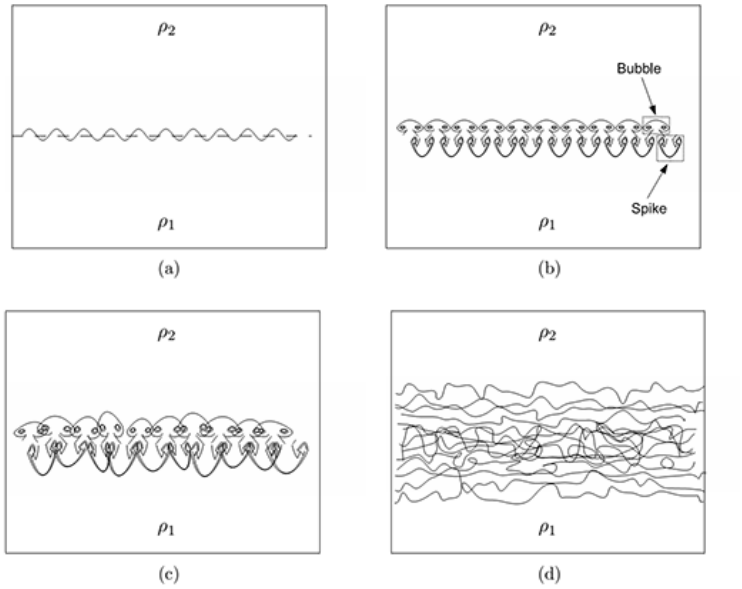

Figure 2.8: Evolution of RTI [29]

The *Kelvin-Helmholtz instability (KHI)* is a fluid instability that occurs when there is either a velocity shear in a single continuous fluid or there is a larger velocity difference across the interface between two fluids. One can often see how the KHI shape the clouds in the sky, or the smoke from a cigarette (see 2.9). The difference in velocity, i.e., the shear flow, results in vorticity at the interface. Due to this the interface becomes an unstable vortex sheet that rolls up into a spiral. This turbulent flow will also result in an increased mixing between the two fluids.

Figure 2.9: Example of Kelvin-Helmholtz Instability [30]

Chapter 3

Methodology

3.1 Experimental setup

Original setup:

The concept behind our experimental setup is much similar to Bjørnsens setup. Her original setup is shown on figure 3.1 below. At the bottom of the setup is a 1/4 inch ball valve (outlet valve) that controls the flow out of the system. Connected to this ball valve is a hose that goes all the way into the flow meter, which is measuring the flow rate and delivering this data to a Pasco IT-system. On the other side of the flow meter is another hose which goes over to a 3m tall acrylic pipe. It is within this acrylic pipe that we are going to look at the displacement of the HOL fluid arrangement. At the beginning of the pipe a pressure sensor has been installed, which is also delivering data to the connected Pasco software. The acrylic pipe itself has a 60mm outer diameter, and 50mm inner diameter. To simulate an actual oil well there has been place another pipe within the previous mentioned acrylic pipe. This is to create the geometry of an annulus. This inner pipe has an outer diameter of 32mm, leaving an annulus with a radius of 18mm. Around 1m under the top of the acrylic pipe is another larger ball valve, which functions as a barrier between the heavy and light fluid until the experiment is initiated. Below the larger ball valve and the acrylic pipe itself (transition between acrylic pipe and hose) there has been placed honeycombs, designed to eliminate any distortion of the flow. 35cm below the larger ball valve there has been placed a "fish tank", a rectangular shaped container, which will help against refraction of light when filming. At the top of the acrylic pipe there has been mounted a y-coupling (overflow safety), which returns any fluid that crosses that height. There are also mounted two hoses. One coming from a sink delivering fresh water. The other coming from a pump, which objective is to pump up the heavier fluid.

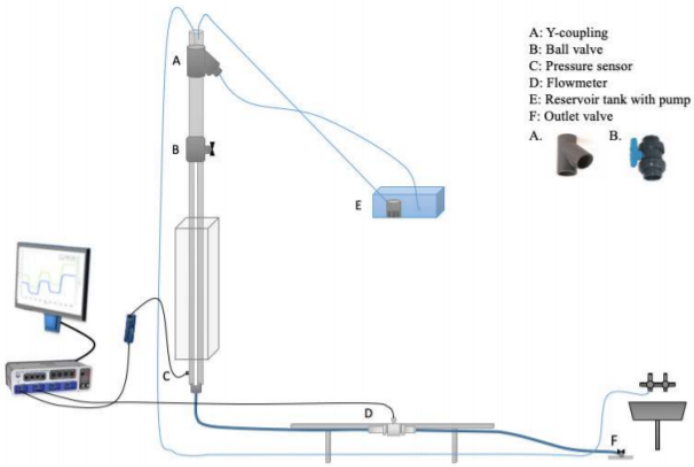

Figure 3.1: Original setup [3]

When the experiments are conducted a black sheet is placed over the setup and camera to remove as much natural lighting as possible. On the backside and on the sides of the fish tank there has been placed cardboard with paper attached to it to create a white background. To be able to fill the fish tank with water and to operate the ball valve at the top, there has been placed a ladder diagonally in front of the setup. It is on this ladder that the camera has been attached (see D.3). When looking through the camera one can see a mirror on the left side. It's been placed there to reflect the light coming from the right side and the rear of the pipe. By doing this we can better understand how the fluid is displaced at different parts of the annulus.

Scaling of original setup: Any structural improvements made to Bjørnsens setup has simply been further added to her original construction. Therefore, much of the scaling of the setup is the same as mentioned in her thesis. Below one find both the scaling of Bjørnsens structure and the scaling of the added structure made by us.

Table 3.1: Relation between actual oil well and experimental setup [3]

Hole section	OD Inner Casing	Ratio
	Typical Oil Well	
17 1/2 inches	13 3/8 inches	1.31
12 1/4 inches	9 5/8 inches	1.27
8 1/2 inches	7 inches	1.21
	Experimental setup	
50mm	32mm	1.56

Table 3.2: Dimensions of experimetnal setup [3]

Parameter	Symbol	Value
Inner diameter of cylinder	ID_C	50mm
Outer diameter of inner pipe	OD_P	32mm
Hydraulic diameter	D_H=ID_C-OD_p	18mm

Improved setup:

It was clear already from the beginning that the setup combined with the sheet, cardboard and camera was not structurally ideal. Due to the non uniform surface of the setup, removing external lighting from outside the sheet proved to be difficult. The sheet also slipped down in front of the camera several times during our early testing, resulting in non-usable results. The sheet was resting on top of the cardboard, which in return made the cardboard unstable. At several points during the testing the cardboard fell down from the original setup. It was clear that the sheet either had to be removed from the cardboard or that a more rigid material had to be placed in the background of the fish tank.

Aluminium profiles: The idea was therefore to build a rigid rectangular frame above the large ball valve, from which three curtains would be attached. Four aluminium profiles were cut, two of them attached to a scaffold that was already set up at the lab, which provided vertical support. Two ropes has also been connected to the corners with no vertical support to give extra structural support. At the top of the frame there has been placed two layers of black sheet to block any external lighting from the top.

As one can see from the pictures in Appendix D (D.3) there is now more room to move around in, making the experiments easier to conduct. Previously the sheet had been placed at a height between the fish tank and the ball valve at the top. To open the ball valve one would therefore have to climb in such a way that you did not disrupt the position of the sheet in. This type of climbing

lead to loss of balance several times and was therefore a potential hazard for injury. With the placement of the curtains and the sheet in the newer setup one can simply climb up and down to the ball valve without having to adjust any grip or balance.

Outlet pipe: The pipe between the flow meter and the outlet valve had been bent over a longer period of time. This had lead to the pipes equilibrium state becoming a curved and dented cylinder shape, instead of providing a straight path for the fluid flow. The original pipe was therefore removed and replaced with a new rigid acrylic pipe.

Lighting: To provide best possible result there has been placed a led strip to the fish tank, directly behind the acrylic pipe (from the cameras point of view). The mirror was placed in such an angle that some of the lighting was from the led strip was directly reflected into the camera. To solve this problem regular paper was taped onto the mirror where the light previously was reflected. The idea of the light strip was taken from Etrati, Alba, and Frigaards report on "Two-layer displacement flow of miscible fluids with viscosity ratio" (2018) [31].

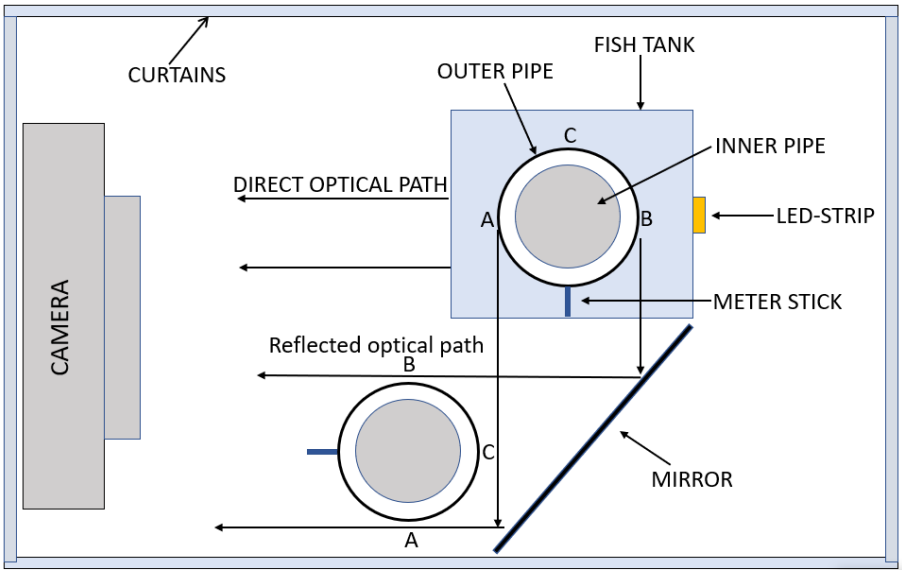

Figure 3.2: Camera setup with LED-strip and curtains

Ink: In Bjørnsens original experiments there was used lissamine red to create colorant. During the replication of her experiments we found that the fluid with added colorant was somewhat transparent. As mentioned in Bjørnsens thesis a better color mixture was needed to achieve clearer results. After receiving a small sample of a water soluble ink we were able to conduct some preliminary tests. We mixed 1ml ink per 1000ml water. In the preliminary tests 5ml of ink were mixed with 5000ml of regular fresh water. As can be seen on the picture below the ink is very potent, and due to it being water soluble it is easy to mix, and also easy to remove when the tests are over.

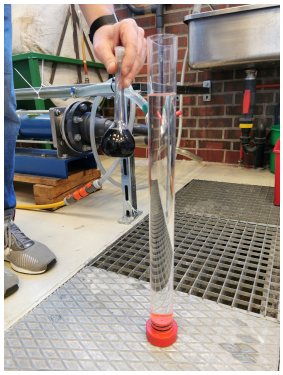

(a) Ink next to test tube

(b) Ink in test tube

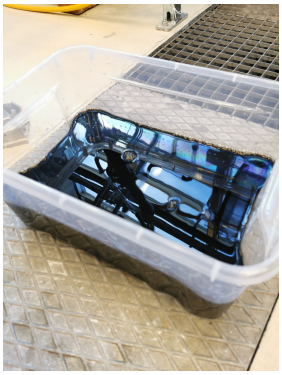

(c) Mixture in container

Figure 3.3: Preliminary testing of ink

3.2 Equipment

Density meter:

To measure the density of the fluids the density meter DMA 4100 M was used. By using the U-tube principle from the producer, Anton Paar, it is able to achieve a precise density with a repeatability of 0.00001 g/cm^3.
With the help of a syringe (no needle attached) one can fill the u-shaped tube that is inside the density meter. With the syringe still in the opening of the density meter to prevent backflow, the measuring of the density may begin. The U-tube which contains the fluid is exposed to small vibration. The U-tube has a resonant frequency that is inversely proportional to the square root of its mass. Because the volume of the tube is known, the density of the fluid filled into the U-tube is calculated from its resonant frequency. To avoid any long term wear on the equipment and to secure its accuracy, the equipment is cleaned after every use. What cleaning agent is best suited depends on the fluid that has been placed inside the U-tube beforehand. In our case with a fluid containing distilled water and ink or lissamin red, distilled water and acetone was used as cleaning agents.

Flow meter

The Endress Hauser Promag 53 Flow Meter used to measure the flow rate. In fact, the flow meter directly measures the voltage created by the fluid passing through a given cross section. One can then calculate the flow rate, as it is proportional to the voltage and the given volume of the cross section. It measures voltage by creating an electromagnetic field within the flow meter. The positively and negatively electrical charged particles in the fluid will then be separated to opposite sides of the inside wall, where there lays two electrodes. These electrodes can pick up and measure electrical voltages. For this particular flow meter to to work it is necessary to have a fluid that contains a certain amount of ions, i.e. a fluid that is conductive. Using non conductive fluid such as oil is therefore not to be recommended for this setup. The adding of impurities (salt and other compounds consisting of ions) to oil may increase the conductivity somewhat.

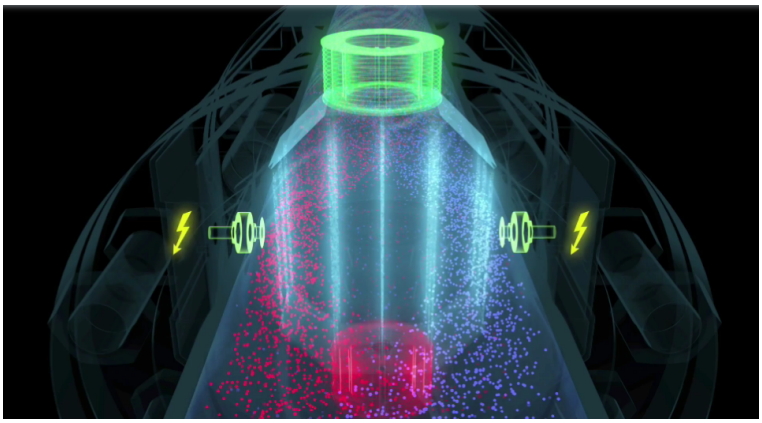

Figure 3.4: Principle of the electromagnetic flow meter

Due to the replacement of the outlet pipe, the flow meter had to be recalibrated (see Appendix A.1).

Pasco:

To measure and store data we used the Pasco Capture software. This software allows us to measure both the voltage from the flow meter and the pressure from the Pasco pressure sensor simultaneously. The data is delivered from an 850 Universal Interface, in which both the Pasco pressure sensor and the flow meter delivers it's data. The flow meter is connected to a Pasco voltage sensor, which again is connected to the 850 universal interace (see D.8).

Weight scale:

To measure the weight of the salt and lissamin red (powder), the Ohaus Adventurer Pro Precision AV4101C was used. It has a repeatability of 0.1g, a margin that was seen as acceptable for this project.

Figure 3.5: Ohaus Adventurer Pro Precision AV4101C

3.3 Procedure

To conduct the experiment with this setup 3 people are recommended. Before running the experiment one should make a heavy fluid mixture ready. In our experiment this heavy fluid consists of distilled water, ink and salt (see A.1 for heavy fluid mix).

To start with, fresh water is pumped through a hose at the top of the rig. Fresh water is first filled almost to the top. To ensure that there is no air trapped in the rig the outlet valve is opened to let any remaining air bubbles out. When the outlet valve is closed the rig is again filled with fresh water, but this time only up to the ball valve. The ball valve is then shut. The pipe collecting the overflow is now placed into the heavy fluid container. Heavy fluid is then pumped up to the 45° y-coupling, where any overflowing heavy fluid will be transported back to the heavy fluid container. When the camera starts recording all participants are in position. Person 1, the person responsible the Pasco Capstone software will now start the measuring. On a countdown Person 2, the person now standing in the ladder in front of the large ball valve, and person 3, the person responsible for the outlet valve, will open both valves at the same time. Person 1 and 3 will further communicate to get a stable and correct outlet flow. Person 2 will climb down the ladder and control the flow from the heavy fluid pump, ensuring that the fluid levels are always at the same level. When the light fluid is fully displaced the camera is shut off and the rig is cleaned by flushing it with fresh water.

Chapter 4

Results and discussion

4.1 Parameters

To ensure the results are as objective as possible a total of 36 runs are accounted for in the results. We will consider 4 flow velocities - 0, 10, 20 and 40mm/s. For each flow velocity we will have 3 runs, resulting in 12 flow varying runs. We will also take into consideration 3 different Atwood numbers. They will also receive 3 runs each at the different flow velocities. Total runs 12·3=36 To get these flow velocities precisely has proven to be difficult as the person opening the outlet valve is depending on receiving ongoing data from the the person responsible for the Pasco Capstone software. Moreover, the time it takes for the change of outlet flow to be registered in the flow meter and transferred to the software creates a delay, which again can affect the accuracy of the flow velocity. In table 4.1 one can see all the average flow velocities.

Table 4.1: Collection of all runs

Series	Flow rate (mm/s)	At	Re	Fr	Re/Fr
1.0.1	-	0.00394	-	-	-
1.0.2	-	0.00394	-	-	-
1.0.3	-	0.00394	-	-	-
1.1.1	10.4	0.00354	281	0.415	676
1.1.2	9.44	0.00354	255	0.377	676
1.1.3	9.62	0.00354	260	0.385	676
1.2.1	18.0	0.00349	486	0.723	671
1.2.2	18.5	0.00349	501	0.746	671
1.2.3	19.5	0.00349	526	0.784	671
1.3.1	34.7	0.00349	983	1.40	671
1.3.2	35.5	0.00349	961	1.43	671
1.3.3	34.8	0.00354	941	1.39	671

2.0.1	-	0.0101	-	-	-
2.0.2	-	0.0101	-	-	-
2.0.3	-	0.0101	-	-	-
2.1.1	9.29	0.0103	254	0.218	1164
2.1.2	9.90	0.0103	270	0.232	1164
2.1.3	10.0	0.0103	273	0.234	1164
2.2.1	25.3	0.0103	689	0.592	1164
2.2.2	21.6	0.0103	589	0.506	1164
2.2.3	21.9	0.0103	597	0.512	1164
2.3.1	44.1	0.0103	1203	1.03	1164
2.3.2	39.8	0.0103	1085	0.932	1164
2.3.3	37.6	0.0103	1026	0.881	1164
3.0.1	-	0.0197	-	-	-
3.0.2	-	0.0197	-	-	-
3.0.3	-	0.0197	-	-	-
3.1.1	10.4	0.0198	288	0.176	1635
3.1.2	10.4	0.0198	287	0.176	1635
3.1.3	10.7	0.0198	295	0.180	1635
3.2.1	22.0	0.0199	608	0.371	1639
3.2.2	22.1	0.0199	610	0.372	1639
3.2.3	19.6	0.0199	542	0.330	1639
3.3.1	40.6	0.0199	1122	0.684	1639
3.3.2	41.7	0.0199	1154	0.704	1639
3.3.3	40.5	0.0199	1119	0.682	1639

From the flowmeter we are given the output Volt. Volt can be converted to flow rate (ml/s) by using the equation created from the calibration of the flowmeter:

$$y = 70.055x - 75.812 \tag{4.1}$$

The flow rate, ml/s, can be converted to flow velocity by using the following equation:

$$v = \frac{Q}{A} = \frac{\pi \cdot Q}{4(ID_C^2 - OD_P^2} \tag{4.2}$$

See Appendix B (B.1) for calibration values.
The values for the Atwood and Froude numbers used in the table 4.1 are the same values used to create the graph 4.1 showing At versus time required to displace, and graph 4.2 showing Fr versus time required to displace. In this project the time required for displacement is defined as the time it takes between the first amount of heavy fluid to be visible on the camera, and until the heavy fluid is the only visible fluid in the annular space.

4.1 Parameters

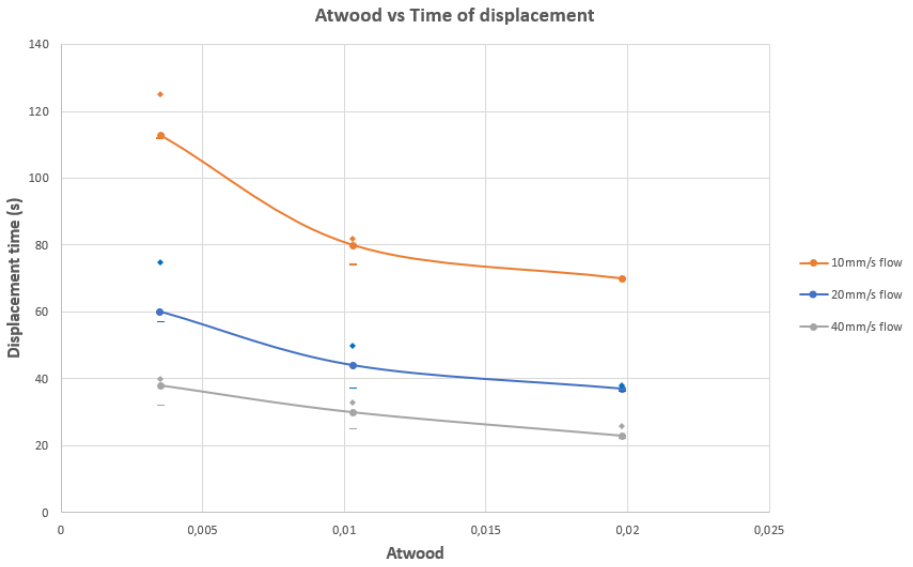

Figure 4.1: Atwood number versus time required for displacement

In the graph above the line goes through the median values. The variation of time at given Atwood numbers are marked with "-" for lower displacement time and a diamond-shaped marker for higher displacement times.

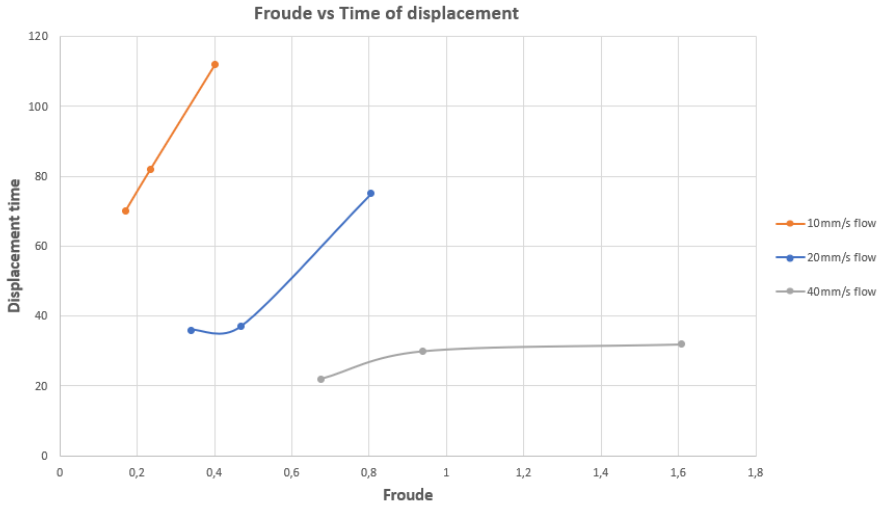

Figure 4.2: Froude number versus time required for displacement

4.1 Parameters

The camera is recording at a frame rate of 60 frames per second. By using a premade script in Matlab one can split the video into 60 pictures per second to better analyze the fluid displacement. We have also used Windows Video Editor for this task. In both the fishtank and on the mirror there has been placed measuring sticks. We can use these to find the distance of penetration of the heavy fluid through the light fluid. In the mirror a clear long plastic rectangle functions as a measuring stick. As one can see on the image below, it has several black markings on it. Between each of these markings there's a 4cm gap.

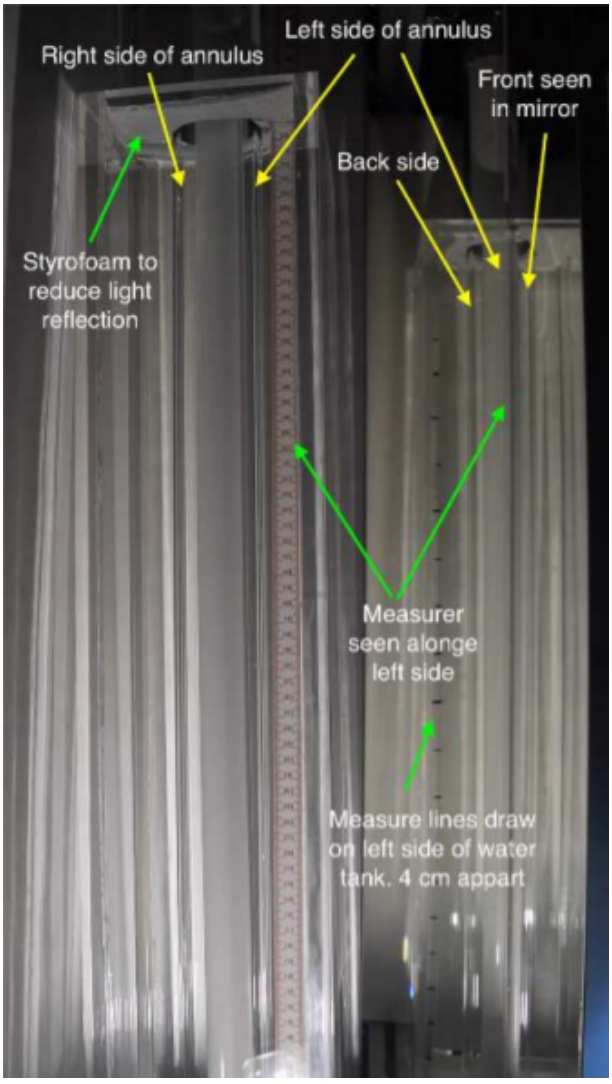

Figure 4.3: Explanation of fish tank and mirror setup [3]

We measure the time to start as soon as the heavy fluid is visible below the ball valve. This may introduce some small margin of error in time measurement. Ideally one could use a tracker software which can detect the change of colour in pixels. This was determined to be too time consuming, but could be used to improve the results even more in further research.

4.2 Analysis of displacement with outlet flow

Below one can see the displacement of the light fluid after a given time of opening the larger ball valve. The frames put next to each other all have the same time and same Atwood numbers, but different flow rate. This is to see how a growing flow rate (Reynolds number) affects the displacement of the light fluid.

At=0.010

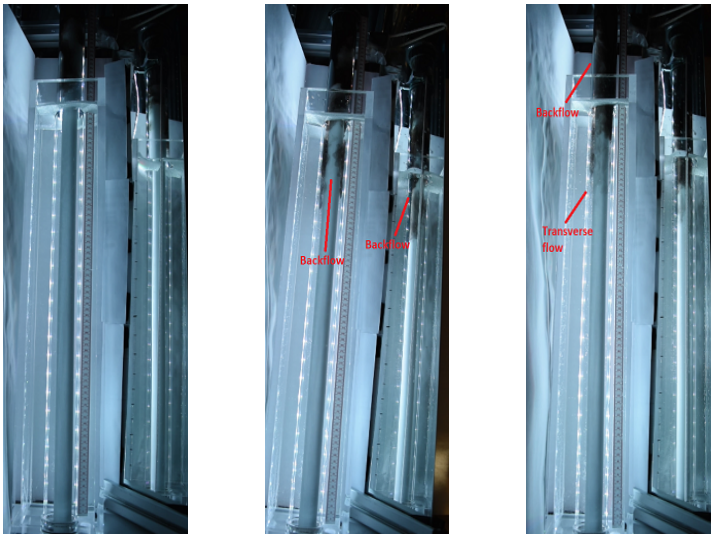

t=5s, v=10mm/s t=5s, v=20mm/s t=5s, v=40mm/s

Figure 4.4: Displacement after 5s - constant At

t=10s, v=10mm/s t=10s, v=20mm/s t=10s, v=40mm/s

Figure 4.5: Displacement after 10s - constant At

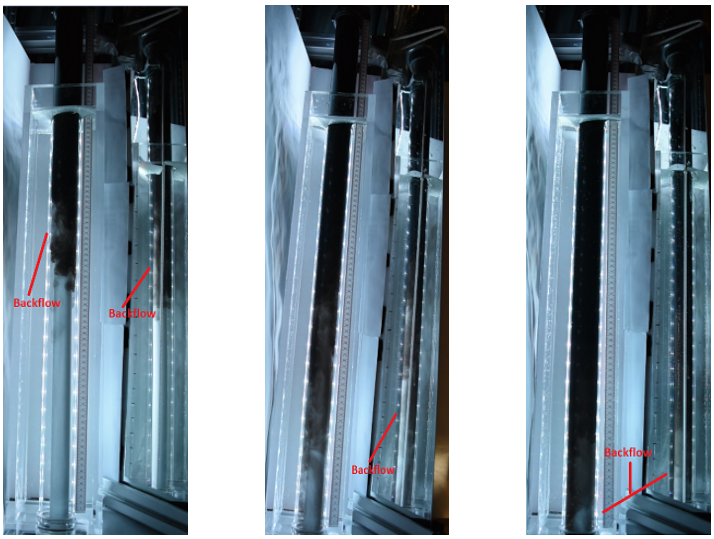

t=20s, v=10mm/s t=20s, v=20mm/s t=20s, v=40mm/s

Figure 4.6: Displacement after 20s - constant At

When increasing the the flow rate one can see more spontaneous and violent mixing at the front. However, overall less upstream flow (backflow) can be seen at higher flow velocities. The downward flow then seems to be the more dominant factor in the system, and as such leads to a better and more time

efficient displacement of the light fluid. This confirms Bjørnsens findings in her 2020 thesis [3]. In the next section of images the flow velocty is now fixed and the Atwood number is varying.

v=20mm/s

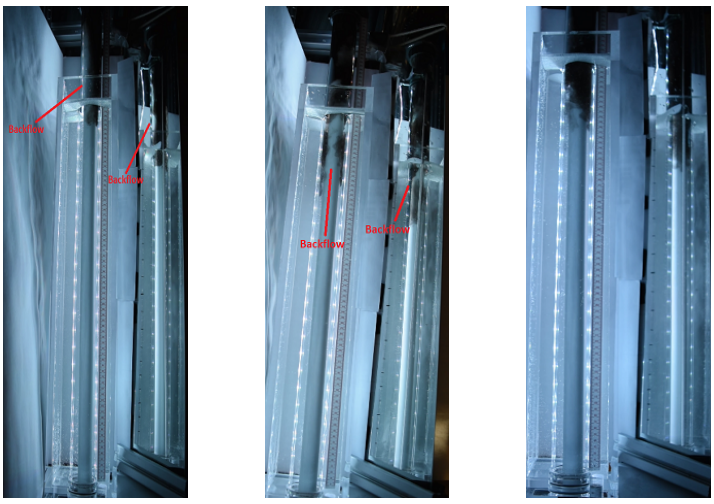

t=5s,At=0.0035 t=5s, At=0.01 t=5s, At=0.02

Figure 4.7: Displacement after 5s - constant flow velocity

t=10s, At=0.0035 t=10s, At=0.01 t=10s, At=0.02

Figure 4.8: Displacement after 10s - constant flow velocity

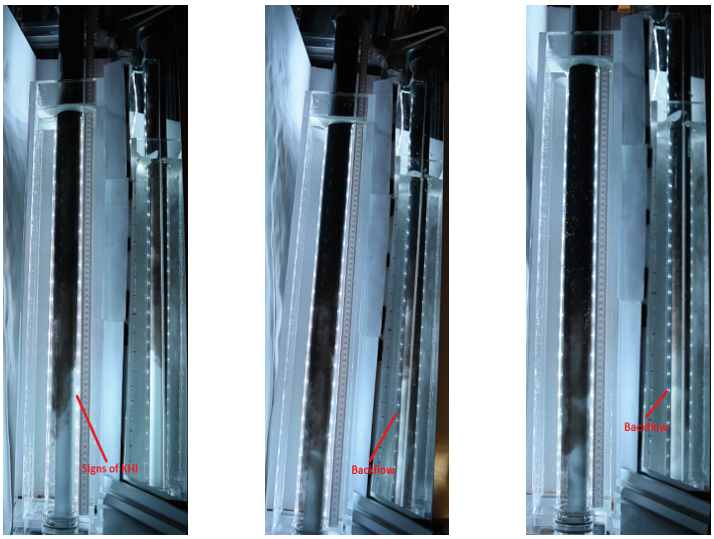

t=20s,At=0.0035 t=20s, At=0.01 t=20s, At=0.02

Figure 4.9: Displacement after 20s - constant flow velocity

As expected, one can see that with increasing Atwood number the time required for displacement becomes smaller.
Due to the eccentricity of the experimental setup it is not a very clear result. However, if we look closer at the pictures with constant flow rate, one can see that with an increasing Atwood number there is also an increased horizontal circular motion (spinning) in the flow. As mentioned earlier this can be caused by the heavy fluid naturally flowing towards the widest part. The energy of this initial rotation against one side of the annulus might be enough to start such spinning. The backflow of the light fluid will therefore also start a spinning motion causing a backflow not just on the narrow side of the annulus, but on all sides. If we are to follow the logic behind equation 2.3, then an increase in Atwood number must increase the penetration depth of the heavy fluid into the light fluid at any given time. Because the outlet flow is constant the only path for the light fluid to travel is upwards (pushed by the heavy fluid). An increase in Atwood number will therefore increase the amount of backflow, unless one has high enough outlet flow velocity to compensate for the increased acceleration of the heavier fluid.
Combining all the results so far one would assume that the best displacement of the light fluid will appear at a lower Atwood number and a higher flow velocity. Following this logic, at a lower Atwood number the acceleration of the heavy fluid is not enough to create any larger mixing due to the downward flow of the system. At the medium and high Atwood number the acceleration of the heavy fluid is high enough to catch up with the outlet flow of the light fluid, and therefore create backflow. One can also see an increasing amount of KHI as the difference in flow velocity between the heavy and light fluid increases. Had the

outlet flow been even higher one could think that our high Atwood number would achieve less backflow then what it does now. In a realistic primary cementing job the well integrity will also have to be considered, meaning an infinite increase of outlet flow and Atwood number is not realistic as it would lead to a dangerously high ECD.

Figure 4.10: High flow & low At VS Low flow & High At

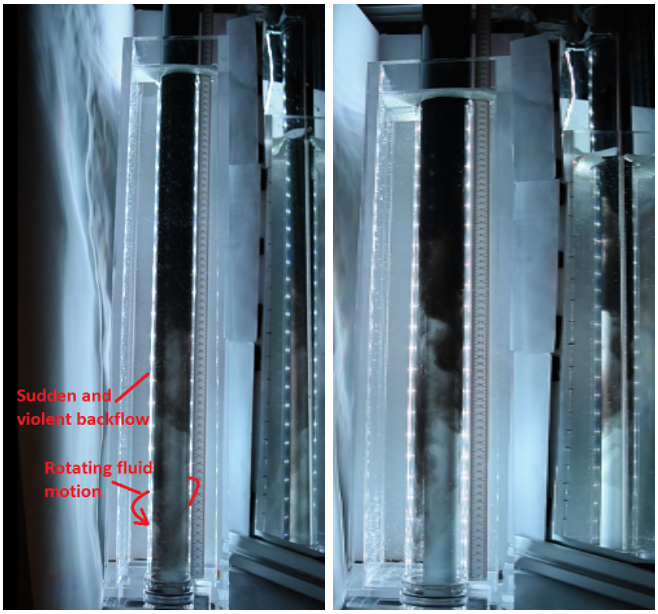

t=36.46s, v=10mm/s, At=0.02 t=15.60s, v=40mm/s, At=0.0035

From the pictures above one can see that although the front of the high velocity, low Atwood-Mixture seems to be less uniform. This non-uniform front is however created at the very start when the large ball valve is opened. Throughout the displacement the heavy fluid seems to sink much more straight down compared to the low velocity, high Atwood-mixture. In that mixture when can see a solid amount of violent backflow as well as much rotating flow. Increasing the flow rate also seems to in this case lead to a better time efficiency than an increased Atwood number. There are also some small variation in the absolute pressure. This is due to the ongoing flow that at times can be hard to control and also depends on the height of the fluid. Any stop in providing ongoing heavy fluid into the system will result in a deviation of the absolute pressure.

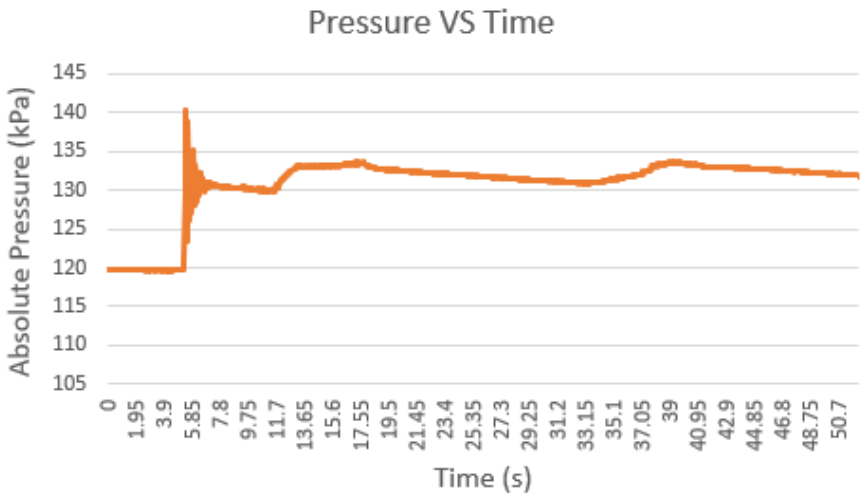

Figure 4.11: Absolute pressure VS time, 20mm/s flow and At=0.02

The graph above is an example of such deviation in the absolute pressure. Ideally it should be similar to 4.16, which shows the absolute pressure vs time with zero flow.

4.3 Analysis of displacement without outlet flow

For this next section you are shown the displacement of the light fluid when the system is not exposed to any outlet flow. The increase in Atwood number and time are the only varying factors taken into account.

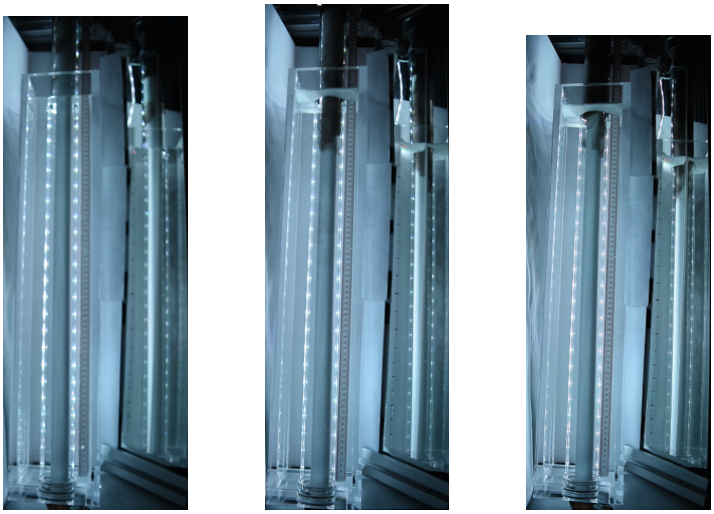

t=50s,At=0.0035 t=50s, At=0.01 t=50s, At=0.02

Figure 4.12: Displacement after 50s - 0 flow

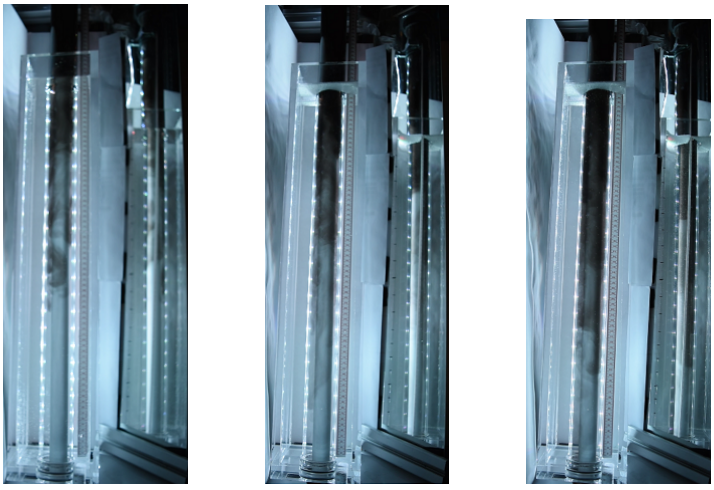

t=70s,At=0.0035 t=70s, At=0.01 t=70s, At=0.02

Figure 4.13: Displacement after 70s - 0 flow

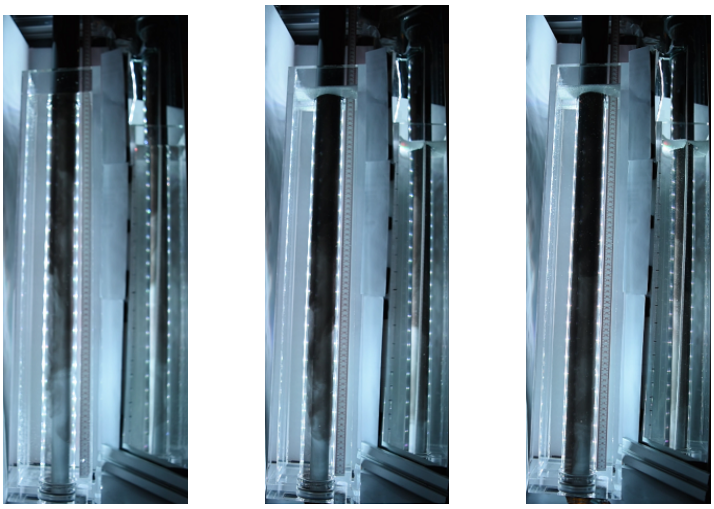

t=120s,At=0.0035 t=120s,At=0.01 t=120s,At=0.02

Figure 4.14: Displacement after 120s - 0 flow

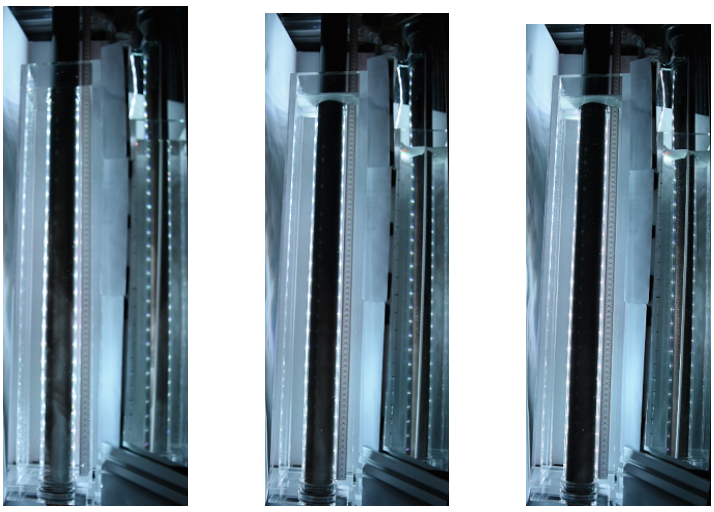

t=240s,At=0.0035 t=240s,At=0.01 t=240s,At=0.02

Figure 4.15: Displacement after 240s - 0 flow

Because there's now no outlet flow, it is clear that Rayleigh-Taylor instability is dominant in the system. There's a lot of mixing for all Atwood numbers. Here we can also see that a higher Atwood number leads to more violent and sudden mixing of the two fluids, but that the displacement itself is also more time efficient. Due to the eccentric annulus we can see that an increase in the density difference also leads to more heavy fluid pushing itself into the front and left

side of the annulus and more of the light fluid is therefore pushed up on the right and back side.

When there's no flow the absolute pressure will not change due to the fact that fluid height is fixed. After the initial opening of the large ball valve the pressure stabilizes after a short period of time, and then remains constant during the rest of the displacement.

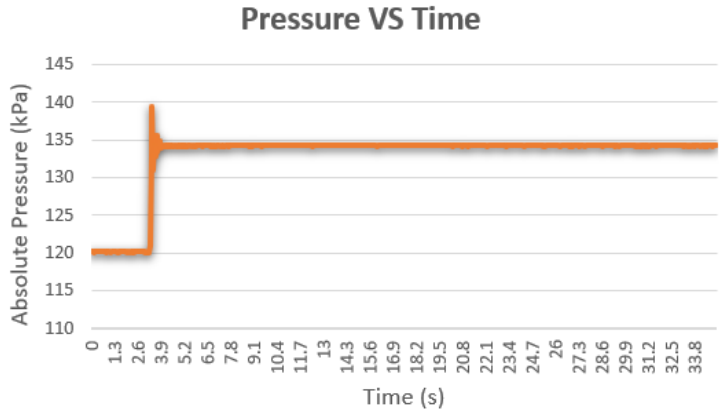

Figure 4.16: Absolute pressure versus time - 0mm/s flow

4.4 Image analysis

By using a Matlab script provided by Professor Rune Wiggo Time (see C.1), one can analyse the displacement of the light fluid by studying the light intensity in each pixel. Below is one image and two graphs describing the movement of the heavy fluid. The graph in the middle describes the movement heavy fluids both directly on top of the red line in the top image (blue line in graph), and also a the movement of the heavy fluid averaged over 61 pixels (orange line in graph); 1 pixel for the red line and 30 pixels on each side of the red line. 1cm equals 24pixels. The black line is used as a reference line and represents the light intensity when there is only fresh water in the annulus

The interval of movement is from image 1257 to 1381 of the video split. Time of initial displacement starts at image 890. Each image is $1/60$ of a second, meaning the interval of movement is from 6.12s to 8.18s.
In this case the system is exposed to an outlet flow of 40mm/s and an At of 0.02.

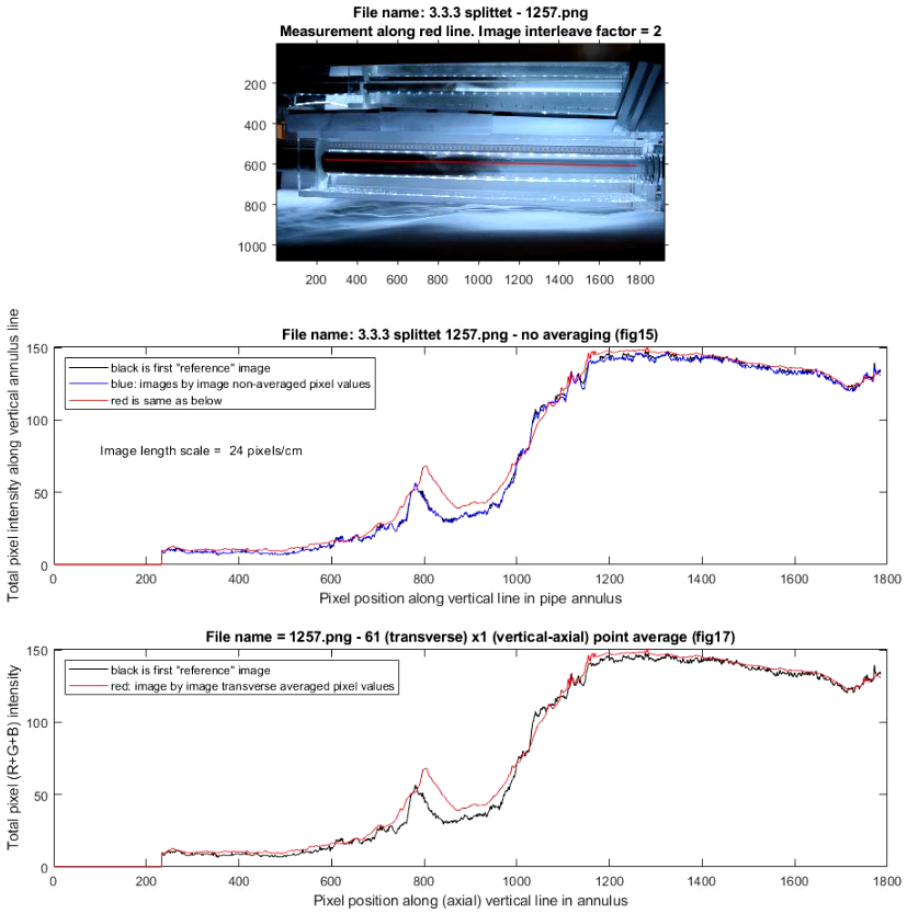

Figure 4.17: Image analysis at 6.12s

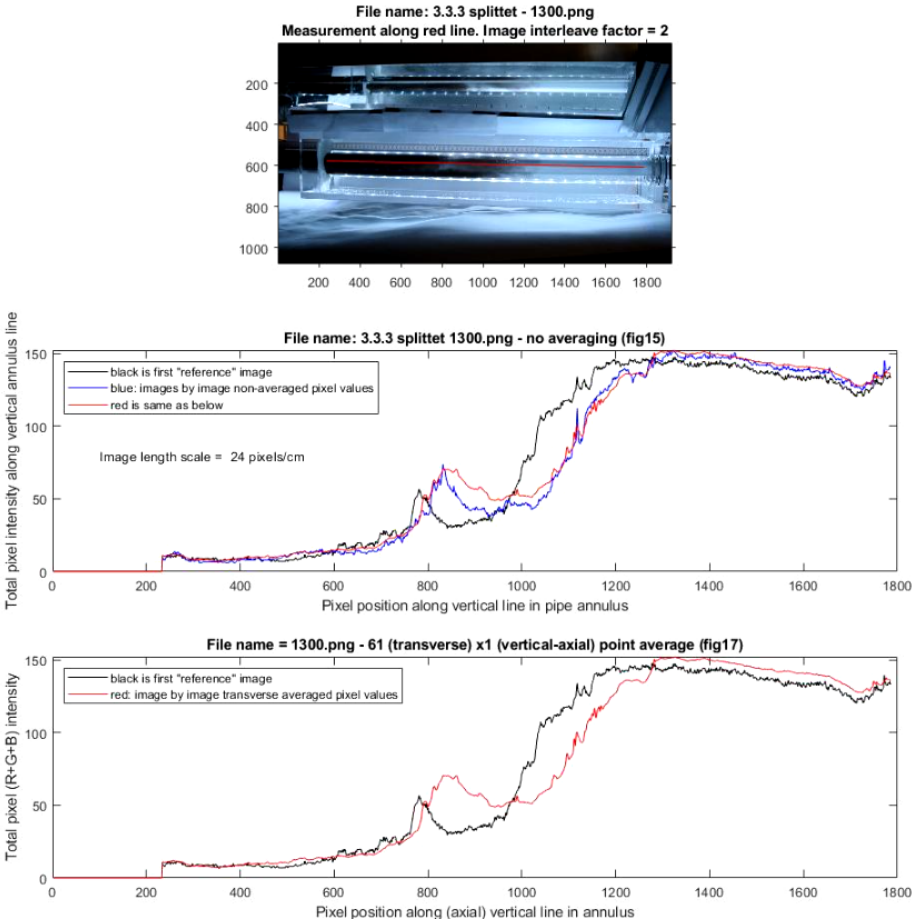

Figure 4.18: Image analysis at t=6.83s

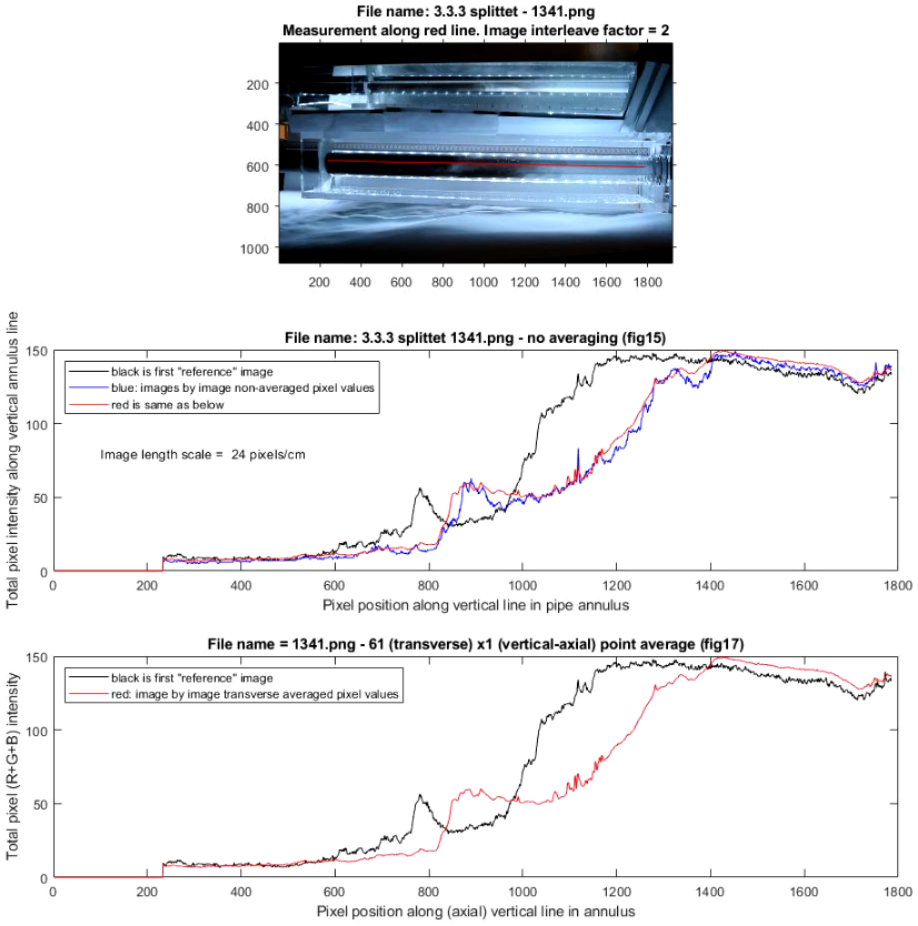

Figure 4.19: Image analysis at t=7.52s

4.4 Image analysis

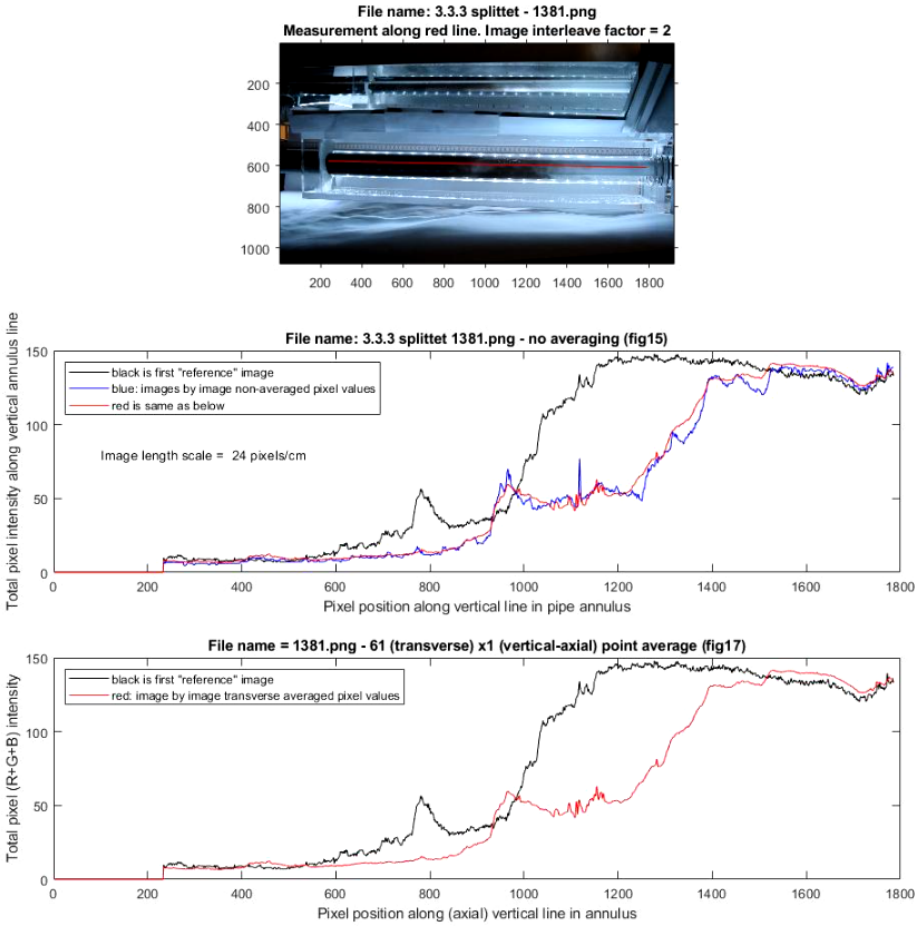

Figure 4.20: Image analysis at t=8.18s

From the figures we can see that the spike in the reference line x=750 to x=800 are transferred to a higher x-value with the orange and blue line. This represents a backflow happening in the referred are. One can also see this backflow on the images placed at the top of the figures. When comparing results proportionally, both for different flow rates and Atwood numbers, one can use such image analysis to determine the difference in backflow and spin. Backflow and spin both has the potential of disturbing a steady decrease of light intensity as the heavy fluid sinks into the light fluid.

Chapter 5

Conclusion

This thesis has focused on improving Bjørnsens [3] work as well as expanding the data. From the results we received it has become clear that an increase in density difference (Atwood number) as well as an increase in flow velocity (Reynolds number) play a larger role in how well the light fluid is displaced in an annulus geometry. It is true that for all runs we have seen some mixing of the fluids, but the size of the mixing and time interval at which this occurs changes with respect to flow velocity and the density difference. For a larger Atwood number one can see that an increased value gives a more violent and sudden backflow. However, this increase in backflow seems to last for a shorter amount of time when compared to a lower Atwood number. It also introduces more spinning in an eccentric annulus due to the amount of energy that naturally starts to flow in the direction of least resistance. When studying the front of the fluid it was found that a higher Atwood number also seemed to expose the fluids for more transverse flow and KHI due to the increased difference in velocity. When looking at the effects of the flow velocity (Reynolds number) it was found that an increased flow velocity resulted in a less uniform front, but at the same time also less backflow and mixing. Even in an eccentric annulus the heavy fluid seemed to flow more vertical when introduced to a high flow velocity. The downward flow (convection term) therefore seems to become the more dominant factor in the system as the fluid velocity increases.

5.1 Recommendation of further work

- Due to the placement of the fish tank we don't get to see the initial contact between the two fluids. The growing chaos in the RT-instability is said to be linear at the very start. Placing the fish tank at the very top would therefore let us see if this is also the case in an annulus geometry.
- As mentioned earlier, a mirror was used to capture the fluid instability from a different angle. It was considered to replace this mirror with a camera identical to the one used in the experiment. This would remove any

image distortion that originates from the mirror. If one chooses to proceed with replacing the mirror with an extra camera, one would encounter other problems such as image synchronization between the two cameras.

- Further work should also consider using a more realistic viscous fluid. An example would be to replace NaCl with sugar which can provide a higher viscosity.
- Detected in the middle of the experimental runs, the annulus is indeed eccentric. To achieve a more fundamental baseline in the research of HOL in annular geometry, making the setup as non-eccentric as possible should be considered.
- Using a Matlab script or a tracker software that detects any change in light intensity will allow more research of the fluid front. It will also give a more objective time stamp for when the displacement starts and ends as well a more objective result of the mixing and backflow.

References

[1] E. Kuru and S. Seatter, "Reverse circulation placement technique vs. conventional placement technique: A comparative study of cement job hydraulics design," pp. 9–16, 2005. [Online]. Available: https://doi.org/10.2118/05-07-TN1.

[2] R. Moore, D. L. Bour, S. Reed, and R. Hernandez, "High-temperature wells with lost-circulation demands and reverse circulation placement technique using foamed cement systems: Two case histories," vol. All Days, Denver, Colorado, USA, Oct. 2003. DOI: 10.2118/84563-MS. [Online]. Available: https://doi.org/10.2118/84563-MS.

[3] C. Bjørnsen, "An experimental investigation of density-unstable displacement in a vertical annulus with relevance to "reverse heavy over light" cementing technology," *University of Stavanger*, 2020. [Online]. Available: https://uis.brage.unit.no/uis-xmlui/handle/11250/2683710.

[4] R. Hernandez and H. Nguyen, "Reverse-circulation cementing and foamed latex cement enable drilling in lostcirculation zones," Apr. 2010. [Online]. Available: https://www.geothermal-energy.org/pdf/IGAstandard/WGC/2010/2137.pdf.

[5] L. Shengtai, "Parallel amr code for compressible mhd or hd equations," p. 1, (accessed: 22.05.2021).

[6] Production Technology, *Casing specification*. [Online]. Available: https://production-technology.org/casing-specifications/, (accessed: 07.05.2021).

[7] M. Khalifeh, "Introduksjon," unpublished, Aug. 2020.

[8] A. W. Mwang'ande, "Evidences of poor cement displacement jobs," pp. 10–11, 2016. [Online]. Available: https://ntnuopen.ntnu.no/ntnu-xmlui/bitstream/handle/11250/2412316/15273_FULLTEXT.pdf?sequence=1&isAllowed=y.

[9] G. Maitland, "Deepwater horizon: As it happened," 2020. [Online]. Available: https://www.thechemicalengineer.com/features/deepwater-horizon-as-it-happened/, accessed: 24.05.2021.

[10] A. W. Khaemba, "Well design, cementing techniques and well work-over to land deep production casings in the menengai field," pp. 304–305, 2014.

[11] (2015). "Cementing job types," [Online]. Available: https://www.drillingcourse.com/2015/12/cementing-job-types.html.

[12] Society of Petroleum Engineers, *Primary cementing placement design*. [Online]. Available: https://petrowiki.spe.org/Primary_cementing_placement_design, (accessed: 10.05.2021).

[13] LIN SCAN, *Caliper (geometry) inspection*. [Online]. Available: https://linscaninspection.com/caliper-geometry-inspection/, (accessed: 10.05.2021.

[14] G. O. Palacio, D. Gardner, L. Delabroy, and A. Govil, "An evaluation of the cement sheath quality of casing sections recovered during a well abandonment operation," Feb. 2020.

[15] D. K. Smith, *Cementing*. Society of Petroleum Engineers of AIME, 1987, vol. 4.

[16] H. J. Skadsem and S. Kragset, "Effect of Buoyancy and Inertia on Viscoplastic Fluid-Fluid Displacement in an Eccentric Annulus With an Irregular Section: Part 2 — Displacements in Vertical Annulus," vol. Volume 8: Polar and Arctic Sciences and Technology; Petroleum Technology, Jun. 2019. DOI: 10.1115/OMAE2019-95700. [Online]. Available: https://doi.org/10.1115/OMAE2019-95700.

[17] *Custom-Blending Foamed Cement for Multiple Challenges*, vol. All Days, SPE/IADC Middle East Drilling Technology Conference and Exhibition, Nov. 1999. DOI: 10.2118/57585-MS. [Online]. Available: https://doi.org/10.2118/57585-MS.

[18] J.Glimm, J. Grove, X. L. Li, W. Oh, and D. H. Sharp, "A critical analysis of Rayleigh–Taylor growth rates," pp. 652–677, 2001. [Online]. Available: https://doi.org/10.1006/jcph.2000.6590.

[19] A. M. Haaland, "Numerical simulation and experimental study of reelwell's heavy over light solution in vertical well sections," *University of Stavanger*, p. 19, 2016. [Online]. Available: https://uis.brage.unit.no/uis-xmlui/handle/11250/2409060.

[20] R. C. Reid, J. M. Prausnitz, and B. E. Poling, *The Properties of Gases and Liquids*. McGraw-Hill Book Company, 1987, p. 433.

[21] Omni calculator, *Water viscosity calculator*. [Online]. Available: https://www.omnicalculator.com/physics/water-viscosityl, (accessed: 07.05.2021).

[22] J. S. Carlton, Fourth edition. Oxford, England ; Cambridge, Massachusetts: Butterworth-Heinemann, 2019.

[23] T. Prešeren, F. Steinman, B. Širok, and T. Bajcar, "The theoretical densimetric froude number values with favourable effect on the clarifier performance," *Chemical Engineering and Processing: Process Intensification*, vol. 74, pp. 97–105, 2013. DOI: https://doi.org/10.1016/j.cep.2013.09.001. [Online]. Available: https://www.sciencedirect.com/science/article/pii/S0255270113001943.

[24] J. Pedlosky, *Geophysical fluid dynamics*. 1987, pp. 10–13.

[25] N. Hall, *Navier-stokes equations*, 2015. [Online]. Available: https://www.grc.nasa.gov/www/k-12/airplane/nseqs.html.

[26] W. L. Hosch, "Navier-stokes equation," *Encyclopedia Britannica*, 2020. [Online]. Available: https://www.britannica.com/science/Navier-Stokes-equation.

[27] A. W. Cook and D. Youngs, "Rayleigh-taylor instability and mixing," *Scholarpedia*, 2009. [Online]. Available: doi:10.4249/scholarpedia.6092.

[28] D. Sharp, "
an overview of rayleigh-taylor instability," *Los Alamos National Laboratory*, 1983. [Online]. Available: https://digital.library.unt.edu/ark:/67531/metadc1104671/m2/1/high_res_d/5913007.pdf.

[29] M. S. Roberts, "Experiments and simulations on the incompressible, rayleigh - taylor instability with small wavelength initial perturbations," *University of Arizona*, 2012. [Online]. Available: https://repository.arizona.edu/handle/10150/265355.

[30] S. Sutherland, "Cloud atlas leaps into 21st century with 12 new cloud types," accessed: 24.05.2021.

[31] A. Etrati, K. Alba, and I. Frigaard, "Two-layer displacement flow of miscible fluids with viscosity ratio: Experiments," *University of British columbia University of Houston*, 2018. [Online]. Available: https://doi.org/10.1063/1.5026639.

[32] R. W. Time, *Example_script_imageanalysis_folder333splittet*, 2021, MatLab.

Appendix A

Heavy fluid mixtures

Table A.1: Specification of heavy fluid

SOLUTION	***DENSITY*** (g/cm^3)	***TEMPERATURE (°C)***	At
1g salt per 100ml fluid	1,0051	20,03	0,00394
1g salt per 100ml fluid	1,0054	20,03	0,00354
1g salt per 100ml fluid	1,0054	20,04	0,00354
1g salt per 100ml fluid	1,0053	20,03	0,00349
1g salt per 100ml fluid	1,0053	20,02	0.00349
1g salt per 100ml fluid	1,0054	20,05	0,00354
3g salt per 100ml fluid	1,0188	20,02	0,0103
3g salt per 100ml fluid	1,0191	19,99	0,0103
3g salt per 100ml fluid	1,0191	20,02	0,0103
3g salt per 100ml fluid	1,0191	20,02	0,0103
3g salt per 100ml fluid	1,0191	20,02	0,0103
3g salt per 100ml fluid	1,0191	20,05	0,0103
6g salt per 100ml fluid	1,0387	20,02	0,0198
6g salt per 100ml fluid	1,0389	20,01	0,0199
6g salt per 100ml fluid	1,0389	20,02	0,0199
6g salt per 100ml fluid	1,0385	20,02	0,0197

Appendix B

Calibration of flow meter

Table B.1: Results from calibration

Test	Volt	Opening (degrees)	Time(s)	Flow (ml/s)
1	1,2100	25,00	558,00	8,96
2	1,3788	30,00	246,00	20,30
3	1,6597	35,00	121,00	41,32
4	1,9875	40,00	79,00	63,29
5	2,1644	40,00	66,00	75,75
6	1,7840	35,00	102,00	49,00
7	1,3680	30,00	253,00	19,76
8	1,1860	25,00	666,00	7,51

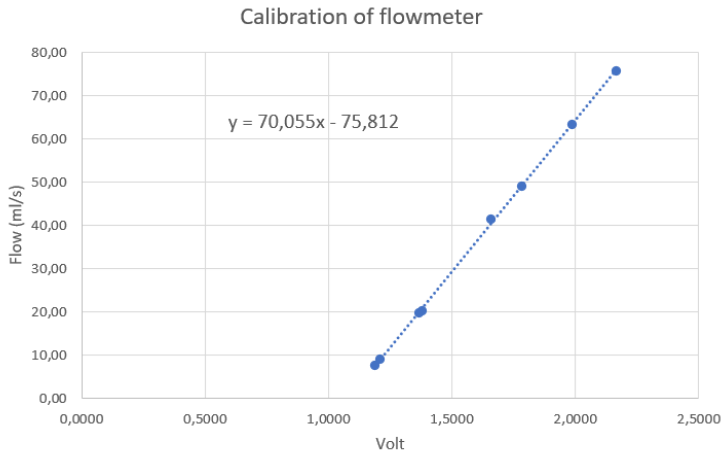

Figure B.1: Graph showing Flow vs Volt during calibration

Appendix C

Image analysis script

Listing C.1: Script of image analysis [32]

```
% Script to read and plot images from folder "3.3.3 splittet"

% This folder name you need to adapt to your own computer:
Foldername= 'C:\Master og bachelor 2021 - pÃ¥ C hjemme\3.3.3 ...
    splittet - fra 1249 - pÃ¥ pc hjemme\'
files = dir(mappenavn) %Reading the file directory

% Make a list of files in your folder, e.g. like here:
for i= 1:20  % Write a list, f.ex from the first 20 files
    % to see that everything is as it should be.
    files(i+8).name
end

% First: Read in and calculate an images colours and position as a
% referance for later images
Name1 = [foldername files(10).name] % Picks out just file number ...
    10 in the list
Image1 = name1 % Original image - name

% Read original images into "bilete"
[bilete, mappe] = imread(bilde1); % Only 8 bit = 255 intensity ...
    values in "bilete"

% Now convert from uint8 to double precision with higher pixel ...
    intensity resolution
DDbilete1 = double(bilete);  %DDbilete1 = Originalbilde ...
    konvertert til double

figure(1)
subplot(2,1,1)
imshow(bilde1) ; % Just to show the original image (uint8 format)

subplot(2,1,2)
imshow(bilete) ; % Double precision format
hold on
```

```
31 % Coordinates for a given analysis line
32 annxtop = 234; annxbot = 1785;
33 annytop = 587; annybot = 617;
34 annxline = [annxtop annxbot];
35 annyline = [annytop annybot];
36 DXann = annxbot-annxtop
37 DYann = annybot-annytop
38
39 title(['Measurement along red line in annulus: (x,y)_{top} = ('...
40 num2str(annxtop) ',' num2str(annytop) '), (x,y)_{bottom} = (' ...
41 num2str(annxbot) ',' num2str(annybot) ').'])
42
43 axis('image')
44 plot(annxline,annyline,'-r')
45 xlabel('x pixel position')
46 ylabel('y pixel position')
47 nn=10
48 FIL = ['File name: 3.3.3 splittet - ' files(nn).name]
49 sgtitle(['Analysis of images.  ' FIL])
50 hold off
```

Appendix D

Photos of setup

Figure D.1: Old setup showing fish tank and camera

Figure D.2: New setup with curtains in front

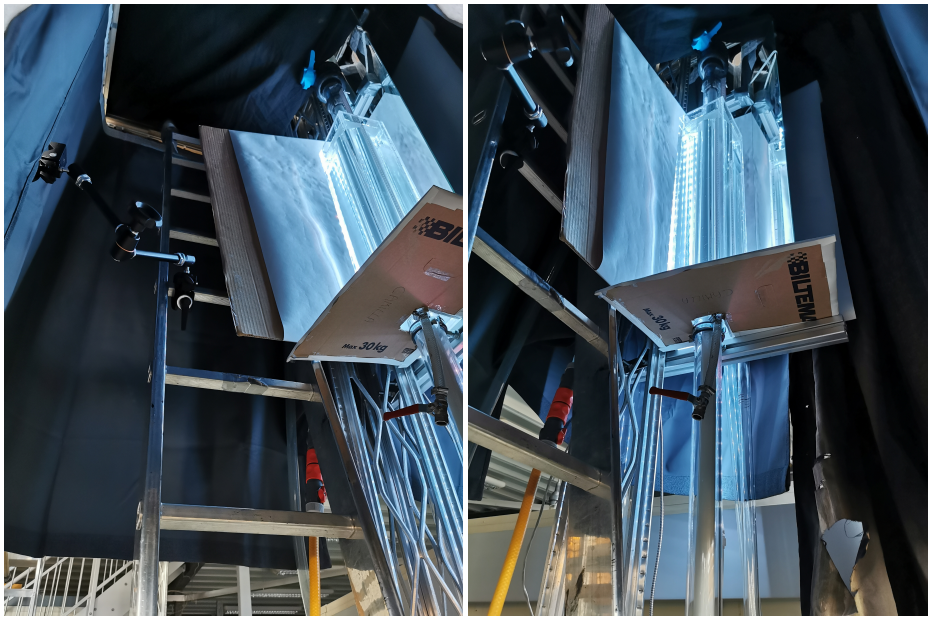

Figure D.3: Inside new setup

Figure D.4: Top of new setup. Curtains laying on top of new metal frame

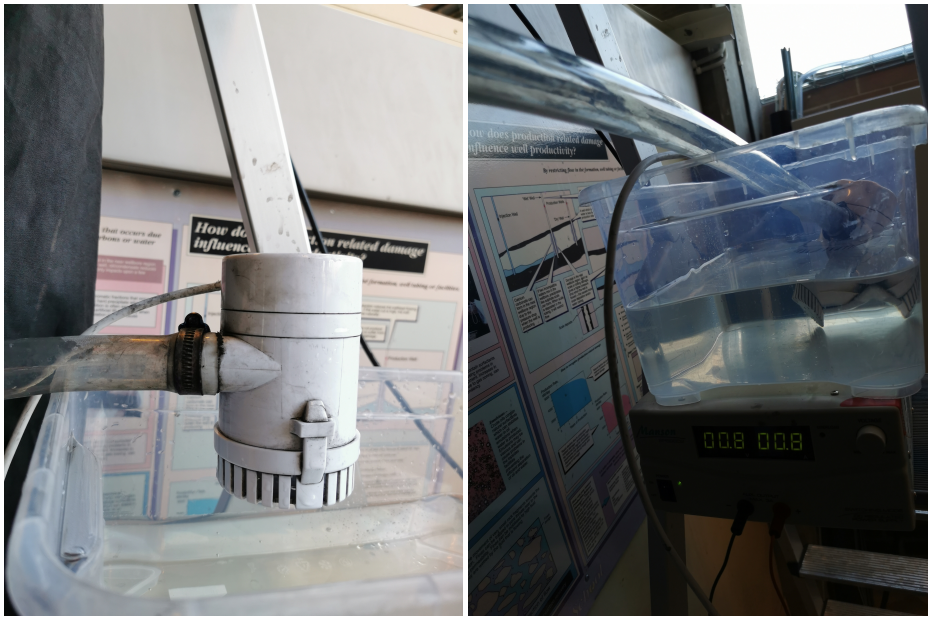

Figure D.5: Pump

Figure D.6: Pasco pressure sensor

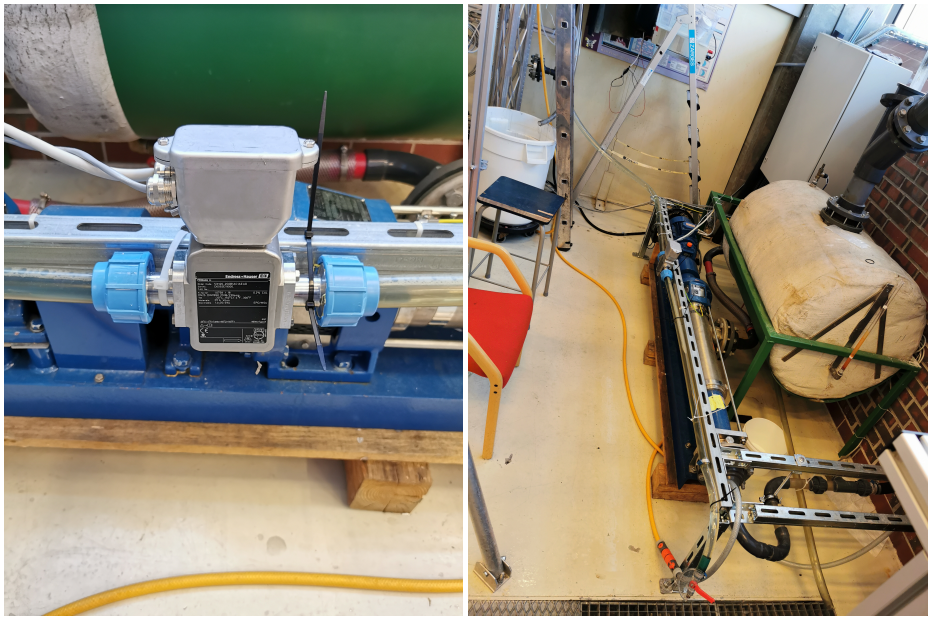

Figure D.7: Flowmeter, outlet pipes, and outlet valve

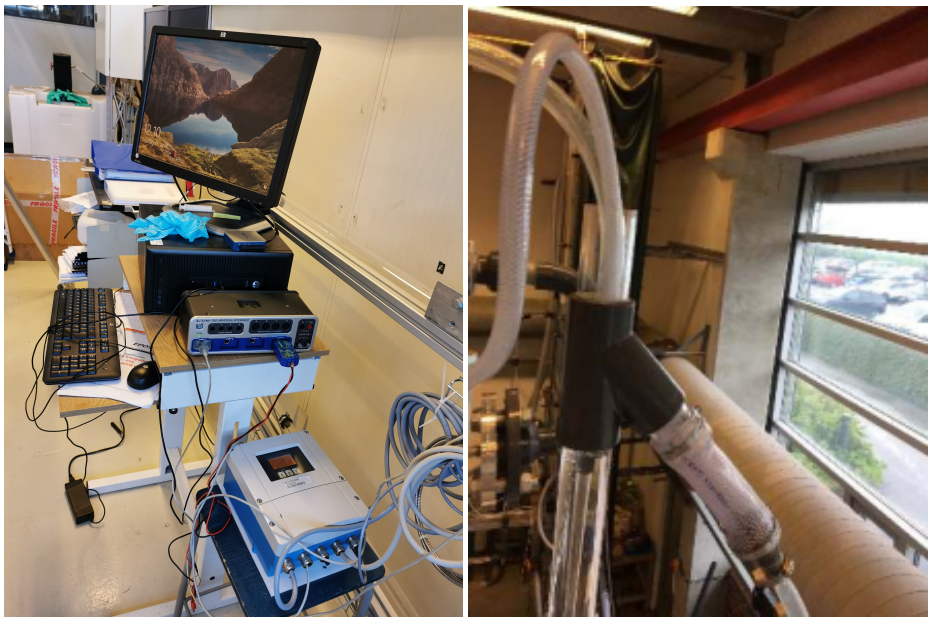

Figure D.8: 45°y-coupling at the top of setup [3] and 850 Universal Interface